

~~Day-night differences in $\delta^{18}\text{O}$ and d -excess~~ Isotopic composition of convective rainfall in the Rio Claro station, inland tropics of Brazil

Vinicius dos Santos¹, Didier Gastmans¹, Ana María Durán-Quesada², Ricardo Sánchez-Murillo³, Kazimierz Rozanski⁴, Oliver Kracht⁵ and Demilson de Assis Quintão⁶.

¹São Paulo State University (UNESP), Environmental Studies Center. Av. 24ABased, 1515, Bela Vista, 13.506-900, Rio Claro, São Paulo, Brazil. vinicius.santos16@unesp.br; didier.gastmans@unesp.br

²Escuela de Física & Centro de Investigación en Contaminación Ambiental & Centro de Investigaciones Geofísicas, Universidad de Costa Rica, San José 11501, Costa Rica. ana.duranquesada@ucr.ac.cr

³University of Texas at Arlington, Department of Earth and Environmental Sciences, 500 Yates Street, Arlington, Texas 76019, USA. ricardo.sanchezmurillo@uta.edu

⁴Faculty of Physics and Applied Computer Science, AGH University of Science and Technology, al. Mickiewicza 30, 30-059 Krakow, Poland. rozanski@agh.edu.pl

⁵International Atomic Energy Agency, Isotope Hydrology Section, Vienna International Centre, P. O. Box 100, 1400 Vienna, Austria. O.Kracht@iaea.org

⁶São Paulo State University (UNESP), IPMet/Science College, Est. Mun. José Sandrin IPMET, S/N, 17.048-699, Bauru, São Paulo, Brazil. demilson.quintao@unesp.br

Correspondence to: Didier Gastmans (didier.gastmans@unesp.br)

Abstract. The tropical central-southern part of Brazil (CSB) is characterized by strong convective systems bringing generous water supply for agro-industrial activities but also pose flood risks for large cities. Here, we present high-frequency (5–10 minutes) rainfall isotopic compositions to better understand those systems, with a total of 90 intra-event samples collected during the period 2019–2021. ~~Convective~~ Combining intra-event and inter-event analysis it is explained how regional and local meteorological processes control the isotope variability within 8 convective rainfall events. While convective activity, associated with outgoing longwave radiation (OLR) and moisture transport, evaluated from Hysplit modelling and ERA-5 eastward vapor flux, modulate the seasonal rainwater isotopic composition with low $\delta^{18}\text{O}$. Low $\delta^{18}\text{O}$ values (median $<-6.8\%$) were observed during summer and, when lower OLR and predominantly moisture influence from Amazon Forest), while high values (median $>-4.2\%$) during autumn and spring. In summer, both regional and local factors contribute to the observed depletion in heavy isotope contents of rainfall, with strong, continuous rainout along the trajectories of moisture-laden air masses arriving at the rainfall collection site from the Amazon basin, and diurnal convective activity of the, when higher OLR and moisture from Atlantic Ocean and South Brazil are acting. A semi-quantitative evaporation model evaluated local atmosphere, respectively. This activity generates influences in summer convective clouds with events revealing distinct features (cloud depth and cloud base height) and induces differences in atmospheric conditions below the cloud base level (relative

Definição de estilo: Texto de comentário

Código de campo alterado

Código de campo alterado

Formatado: Inglês (Reino Unido)

Formatado: Inglês (Reino Unido)

Formatado: Inglês (Reino Unido)

Formatado: Inglês (Reino Unido)

Formatado: Inglês (Reino Unido)

35 ~~humidity and rainfall rates) modifying isotopic isotope characteristics of rainfall between day (high $\delta^{18}\text{O}$, low d -excess and revealing novel perspective on day-substantial evaporation) and night contrast in $\delta^{18}\text{O}$ and d -excess values. During daytime, enhanced sub-cloud effects lead to high $\delta^{18}\text{O}$ and (low d -excess while continuous regional rainout during night time results in low $\delta^{18}\text{O}$ and $\delta^{18}\text{O}$, high d -excess values of local rainfall and negligible evaporation).~~ Our results offer a new framework of key drivers controlling the isotopic variability of rainfall in tropical South America that must be considered in future studies of convective systems across the tropics.

40 1_ Introduction

The central-southern part of Brazil (CSB) is the main contributor to the Brazilian economy, with agriculture and industry as leading activities (Zilli et al., 2017). These sectors strongly depend on rainfall seasonality for irrigation and hydropower supply (Luiz Silva et al., 2019). Suggested changes in frequency of heavy and extreme rainfall events in future climate scenarios (Marengo et al., 2020; Donat et al., 2013; IPCC, 2021) may represent a serious threat to regional economic activities and electricity generation. Similarly, climate projections also suggest that enhancement of heavy rainfall events will aggravate the occurrence of both floods and landslides across vulnerable areas (Marengo et al., 2020), whose total cost has risen to US\$ 41.7 billion in the past 50 years (Marengo et al., 2020; World Meteorological Organization, 2019,2021).

45 Extreme rainfall events are related to the convective systems (CS), characterized by strong vertical development in the form of *cumulus-nimbus* and *cumulus congestus* (convective clouds) and low-level ~~convergence~~divergence (stratiform clouds) (Siqueira et al., 2005; Machado and Rossow, 1993; Zilli et al., 2017)(Siqueira et al., 2005; Machado and Rossow, 1993; Zilli et al., 2017; Houze, 1989, 2004), commonly refer to as convective and stratiform rainfall, that account for 45% and 46% of the total rainfall in South America, respectively (Romatschke and Houze, 2013). These rainfall types have recently been postulated as a major driver explaining variations in stable isotope composition of precipitation across the tropics (Zwart et al., 2018; Sánchez-Murillo et al., 2019; Sun et al., 2019; Han et al., 2021; Aggarwal et al., 2016). Specifically, the role of tropical convection in formation of the isotopic composition of rainfall has been discussed in the context of so-called- amount effect (heavy isotope contents of tropical precipitation decrease as the amount of local precipitation increases) (Dansgaard, 1964; Hu et al., 2018; Kurita, 2013a; Rozanski et al., 1993; Winnick et al., 2014; Tharammal, T., G. Bala, 2017)(Dansgaard, 1964; Hu et al., 2018; Kurita, 2013; Rozanski et al., 1993; Winnick et al., 2014; Tharammal, T., G. Bala, 2017).

55 Previous studies used satellite retrievals of atmospheric water vapor isotopic composition to better understand convective processes in other regions (Lawrence et al., 2004; Worden et al., 2007; Kurita, 2013b). ~~They showed the links between the structure and depth of convective systems; and variations in the isotopic composition of local vapor, being strongly depleted in ^{18}O with for deep convection systems. Consequently, similar relations were observed for local rainfall, confirming the important role of convection systems in reducing heavy isotope contents of precipitation in the tropics(Lawrence et al., 2004; Worden et al., 2007; Kurita, 2013). They showed the links between the structure and depth of convective systems as well as variations in the isotopic composition of local vapor (Lekshmy et al., 2014; Vuille et al., 2003; dos Santos et al., 2022)(e.g.~~

Código de campo alterado

[Lekshmy et al., 2014](#); [Vuille et al., 2003](#); [dos Santos et al., 2022](#)). Despite these advances, to date only few studies have examined the rainfall isotopic composition in the light of diurnal variations in convective activity of tropical atmosphere (Munksgaard et al., 2020; Moerman et al., 2013).

Diurnal variations in heating of the surface intensify convection processes, generating short-lived events that can occur in consecutive days across the tropics (Romatschke and Houze, 2013, 2010). These events are characterized by a diurnal cycle and notable differences in: (i) rainfall intensity, (ii) vertical extent of convective cores between deep and shallow convection, and (iii) life cycle of these events in ~~Mesoseale Convective Systems~~ [mesoscale convective systems](#) (MCSs) (Schumacher and Houze, 2003; Romatschke and Houze, 2013, 2010). ~~Convective events account for a significant proportion of annual rainfall and are linked with extreme events over the land, with most intense events occurring in the afternoon~~ (Schumacher and Houze, 2003; Kurita, 2013a; Wang and Tang, 2020). ~~Convective events account for a significant proportion of annual rainfall and are linked with extreme events over the land, with most intense events occurring in the afternoon~~ (Schumacher and Houze, 2003; Kurita, 2013; Wang and Tang, 2020). High-frequency rainfall sampling strategies during the occurrence of convective events are needed to capture the diurnal heating cycle and associated variations in the isotopic signatures of convective rainfall.

High-frequency rainfall sampling and analyses of stable isotope ratios has been used to better understand the evolution of large ~~atmospheric weather~~ systems such as tropical cyclones and typhoons (Sun et al., 2022; Sánchez-Murillo et al., 2019; Han et al., 2021), ~~squall lines~~ (Taupin et al., 1997; Risi et al., 2010; Tremoy et al., 2014) and local evaporation effects (~~Graf et al., 2019; Aemisegger et al., 2015b; Lee and Fung, 2008~~). (Graf et al., 2019; Aemisegger et al., 2015; Lee and Fung, 2008). This high-resolution isotope information provided a better insight into the development of weather systems and cloud dynamics, both responsible for changes in the rain type, intensity, and inherent isotope variability during rainfall events (Coplen et al., 2008; Muller et al., 2015; Celle-Jeanton et al., 2004). ~~However~~ ~~Nevertheless~~, high-frequency isotope sampling of rainfall has been limited across the tropics, despite convective activity being significant in this region.

Using high-frequency rainfall sampling strategy we focus here on processes controlling isotopic composition of ~~rainwater on diurnal time scale~~ [convective rainfall](#), which are of local (below-cloud evaporation and [isotope](#) exchange processes, vertical structure of rainfall, cloud top over sampling site, and others) and regional (moisture origin/transport, regional atmospheric circulation, ~~and convective activity~~). ~~Evolution of convection systems on the diurnal cycle is used here only to characterize the clouds during day and night situations.~~ We combine high-frequency rainfall sampling with ground-based observational data (Micro Rain Radar, and automatic weather station) with satellite imagery (GOES-16), ERA-5 reanalysis products and HYSPLIT trajectories to ~~study the day-night differences in isotopic composition of~~ [characterize](#) convective rainfall collected over the inland tropics of Brazil.

95 2 Data and Methods

2.1 Sampling site and atmospheric weather systems

The rainfall sampling site was localized in Rio Claro city, São Paulo State (Fig. 1a). The station (-22.39°S, -47.54°W, 670 m.a.s.l.) belongs to Global Network of Isotopes in Precipitation network (GNIP) and is influenced by atmospheric weather systems responsible for rainfall variations and seasonality linked to the regional atmospheric circulations of CSB region. The rainfall seasonality over CSB is associated with: (i) Frontal Systems~~frontal systems~~ (FS), represented mainly by Cold Fronts~~cold fronts~~ from southern South America (SA) acting all the year, and (ii) the South Atlantic Convergence Zone (SACZ) during austral summer (December to March) (Kodama, 1992; Garreaud, 2000) (Fig. 1b). These synoptic features are mostly responsible for the development of CS (Romatschke and Houze, 2013; Siqueira et al., 2005; Machado and Rossow, 1993) (Fig. 1c), and were captured during their passage over the Rio Claro station.

105 2.2 Rainfall sampling and isotope analyses

High-frequency sampling of rainfall events was done manually with the aid of passive collector (ca. 2 to 10 minutes intervals) from September 2019 to February 2021, except for April, July, and August (during winter 2020), when no rainfall was observed in the study area. Due to the difficulties of manual sampling and uncertainties involved in forecast of rainfall occurrences for one point, rainfall events were collected randomly during the monitoring period. Covid-19 restricted access at the university, which resulted in fewer rainfall events sampled, mainly at night during spring-2020. The rainfall samples collected in this study generally do not represent consecutive pairs of day-night data during the same day. Rainwater was manually collected with a passive collector at 5-10 minutes intervals, from September 2019 to February 2021, except for April, July, and August 2020, when no rainfall was observed in the study area (Fig. 2). Due to the difficulties of manual sampling and complexity in forecast rainfall occurrences for one point, rainfall events were collected randomly during the monitoring period. Rainfall samples (n=90) were immediately transferred and stored in 20 mL HDPE bottles with sealed caps. Air bubbles were avoided to prevent potential isotopic exchange with the headspace and fractionation.

Daytime data are related to rainfall samples collected at Rio Claro station from 07:00 to 18:59 local time (10:00-21:59 UTC) whereas night-time data represent the period 19:00-06:59 local time (22:00-09:59 UTC). In total, 90 samples representing eight convective events (3 night-time events and 5 day-time events) have been collected. The collected samples were transferred to the laboratory and stored in 20 ml HDPE bottles at reduced temperature (+4°C). In parallel to high-frequency sampling, monthly cumulative rainfall samples were also collected at the Rio Claro site during the study period as a contribution to the GNIP network, using the methodology recommended by the International Atomic Energy Agency (IAEA, 2014).

2.3 Isotope analyses

125 Rainfall samples were analysed for stable isotope composition using Off-Axis Integrated Cavity Output Spectroscopy (Los
Gatos Research Inc.) at the Hydrogeology and Hydrochemistry laboratory of UNESP's Department of Applied Geology and
at the Chemistry School of the National University (Heredia, Costa Rica). All results ~~were~~are expressed in per mil relative to
Vienna Standard Mean Ocean Water (V-SMOW). The certified calibration standards used in UNESP were USGS-45 ($\delta^2\text{H} =$
130 -10.3‰ , $\delta^{18}\text{O} = -2.24\text{‰}$), USGS-46 ($\delta^2\text{H} = -236.0\text{‰}$, $\delta^{18}\text{O} = -29.80\text{‰}$), including one internal standard (Cachoeira de Emas
- CE - $\delta^2\text{H} = -36.1\text{‰}$, $\delta^{18}\text{O} = -5.36\text{‰}$). USGS standards were used to calibrate the results on the V-SMOW2-SLAP2 scale,
whereas CE was used for memory and drift corrections. In Costa Rica laboratory, the certified standards MTW ($\delta^2\text{H} =$
 -130.3‰ , $\delta^{18}\text{O} = -16.7\text{‰}$), USGS45 ($\delta^2\text{H} = -10.3\text{‰}$, $\delta^{18}\text{O} = -2.2\text{‰}$), and CAS ($\delta^2\text{H} = -64.3\text{‰}$, $\delta^{18}\text{O} = -8.3\text{‰}$) were used
to correct the measurement results for memory and drift effects and to calibrate them on the V-SMOW2-SLAP2 scale (García-
Santos et al., 2022). The analytical uncertainty (1σ) was $\pm 1.2\text{‰}$ (~~+ σ~~) for $\delta^2\text{H}$ and $\pm 0.2\text{‰}$ (~~+ σ~~) for $\delta^{18}\text{O}$ for UNESP analysis
135 and 0.38‰ for $\delta^2\text{H}$ and 0.07‰ for $\delta^{18}\text{O}$ and 0.38‰ $\delta^2\text{H}$ for Costa Rica analysis. Deuterium excess (d -excess) was calculated
as: $d\text{-excess} = \delta^2\text{H} - 8 \cdot \delta^{18}\text{O}$ (Dansgaard, 1964). Its uncertainty $1(\sigma)$ resulting from the uncertainties of the isotope analyses
was equal 1.33 and 0.43‰, respectively. This secondary isotope parameter was used to interpret the influence of moisture
origin/transport (Sánchez-Murillo et al., 2017; Froehlich et al., 2002) and to quantify below-cloud processes (e.g. Jeelani et
al., 2018; Graf et al., 2019; Aemisegger et al., ~~2015b~~2015).

140 2.3.4 Meteorological data

Automatic Weather Station (AWS) Decagon Em50 (METER) was installed near the Micro Rain Radar (MRR) (METEK)
at 670 m.a.s.l, in immediate vicinity of the rainfall collection site. Meteorological data were recorded at 1 min intervals for
rain rate (AWS RR, $\text{mm}\cdot\text{min}^{-1}$), air temperature (T, $^{\circ}\text{C}$), and relative humidity (RH, %) and pressure (kPa).%. The MRR data
for reflectivity (Z, dBZ), and fall velocity (w, $\text{m}\cdot\text{s}^{-1}$), liquid water content (LWC, $\text{g}\cdot\text{m}^{-3}$) and rain rate (MRR RR, $\text{mm}\cdot\text{min}^{-1}$)
145 were also recorded at 1 min intervals. MRR parameters correspond to the mean values measured at the elevation between 150
and 350 meters above the local ground. MRR operated at a frequency of 24.230 GHz, modulation of 0.5 – 15 MHz according
to the height resolution mode. For this work, different height resolutions (31 range bin) were tested, 150m, 200m, 300m and
350m, resulting in vertical profiles of 4650m, 6200m, 9300m and 10.850m, respectively (Endries et al., 2018). The MRR data
used in the following discussion are the near-surface data (first measurement from 150m to 350m). The MRR vertical profile
150 (from 150m to 10.850m) was used to classify and visualize the radar echoes. Rain rates (AWS and MRR) were computed for
5 min intervals ($\text{mm}\cdot 5\text{min}^{-1}$) following the chosen interval of isotope rainfall sampling. Lifting Condensation Level (LCL,
meters) was computed from AWS RH and T, following using expression proposed by Soderberg et al. (2013).

GOES-16 imagery (https://home.chpc.utah.edu/~u0553130/Brian_Blalock/cgi-bin/goes16_download.cgi) was used to
identify the convective nuclei of the cloud-top (10.35- μm , Band-13) and brightness temperature (BT), at 10 min intervals

Formatado: Recuo: Primeira linha: 0 cm

Formatado: Inglês (Estados Unidos)

Código de campo alterado

Formatado: Francês (França)

Formatado: Recuo: Primeira linha: 0.5 cm

Formatado: Sobrescrito

155 during the sampling period ~~over the Rio Claro station~~ (Ribeiro et al., 2019; Schmit et al., 2017). The 10.35- μm BT is often used to estimate the convective cloud depth, since the lower BT is linked to deeper cloud tops (Adler and Fenn, 1979; Roberts and Rutledge, 2003; Adler and Mack, 1986; Ribeiro et al., 2019; Machado et al., 1998).

The weather systems (Frontal, instabilities and low pressure) were defined according to the synoptic chart (<https://www.marinha.mil.br/chm/dados-do-smm-cartas-sinoticas/cartas-sinoticas>) and meteorological technical bulletin of the Center for Weather Forecast and Climatic Studies of the National Institute of Space Research (CPTEC/INPE: (<http://tempo.cptec.inpe.br/boletimtecnico/pt>) that used information of numerical model, modern observation systems, automatic weather stations, satellite and radar images, reanalysis data and regional atmospheric models, such as the Brazilian Global Atmospheric Model and ETA model.

2.5. Hysplit modelling and reanalysis data

165 The origin of air masses and moisture transport (~~Fig. 1e~~) to the Rio Claro site were ~~analysed~~evaluated using the HYSPLIT ~~Model~~(Hybrid-Single Particle Lagrangian Integrated Trajectory) modelling framework (Stein et al., 2015; Soderberg et al., 2013). ~~Trajectories of convective events were estimated for t-240 hours prior to rainfall collection and ending elevations at 1500m above the surface, following (dos Santos et al., (2022)). The meteorological outputs: heights (meters), relative humidity (%), and rainfall intensity ($\text{mm}\cdot\text{hr}^{-1}$) along the trajectories were used to analyse the rainout processes.~~The trajectories of the air masses were estimated for 240 hours prior to rainfall onset, considering the estimated time of residence of the water vapor (Gimeno et al., 2010, 2020; van der Ent and Tuinenburg, 2017). Start time of trajectories was the same as the start time of rainfall events. The trajectories were computed using NOAA's meteorological data (global data assimilation system, GDAS: 1 degree, global, 2006-present), with ending elevations of the trajectories at 1500 m above the surface, taking into account the climatological height of the Low Level Jet, within 1000–2000 m (Marengo et al., 2004). Ten-day trajectories representing convective events were calculated as trajectory ensembles, each consisting of twenty-seven ensemble members released at start hour of convective rainfall sample collection. Ensembles were produced by varying the initial trajectory wind speeds and pressures, according to the HYSPLIT ensemble algorithm, in order to account for the uncertainties involved in the simulation of individual backward trajectories (Jeelani et al., 2018).

175 Reanalysis data were used to better understand the influence of atmospheric circulation on isotopic composition of rainfall at the study area. ERA-5 climatology (<https://cds.climate.copernicus.eu/cdsapp#!/search?type=dataset>) was used to generate plots of hourly vertical integral of eastward water vapor flux during convective events sampled. The Global Modelling and Assimilation Office (GMAO) data (MERRA-2, 1 hour, 0.5 x 0.625 degree, V5.12.4 - <https://goldsmr4.gesdisc.eosdis.nasa.gov/data/MERRA2/M2T1NXFLX.5.12.4/>) were used for calculations of latent heat flux (LHF), and Aqua/AIRS L3 Daily Standard Physical Retrieval (AIRS-only) 1 degree x 1 degree V7.0, Greenbelt, MD, USA, Goddard Earth Sciences Data and Information Services Center (GES DISC) data, were used for average outgoing longwave radiation (OLR) (https://disc.gsfc.nasa.gov/datasets/AIRS3STD_7.0/summary). OLR values below $240\text{W}\cdot\text{m}^{-2}$ indicate

Formatado: Fonte: 12 pt, Inglês (Estados Unidos)

Formatado: Recuo: Primeira linha: 0 cm

190 organized deep convection (Gadgil, 2003). Global Land Data Assimilation System Version 2 (GLDAS-2) Noah Land Surface Model L4 3 hourly 0.25 x 0.25 degree V2.1, Greenbelt, Maryland, USA, Goddard Earth Sciences Data and Information Services Center (GES DISC) were used for calculations of evapotranspiration (https://disc.gsfc.nasa.gov/datasets/GLDAS_NOAH025_3H_2.1/summary). A 10-day mean evapotranspiration values (mm) were computed based on the back hour (240 hours) and coordinates (latitude e longitude) of HYSPLIT trajectories.

2.4 Convective-6 Identification of convective rainfall classification events

195 In General, classification general, identification of convective precipitation systems was based on the vertical structure of the given precipitation system (lack of the melting layer and bright band - BB) in the radar profiles featuring high reflectivity values ($Z > 38$ dBZ) (Houze, 1993, 1997; Steiner and Smith, 1998; Rao et al., 2008; Mehta et al., 2020; Endries et al., 2018) and satellite imagery (Vila et al., 2008; Ribeiro et al., 2019; Siqueira et al., 2005; Machado et al., 1998). Consequently, convective rainfall was defined in this study by (i) convective cloud nuclei observed in GOES-16 imagery, (ii) no BB detected, (iii) $Z > 38$ dBZ near-near to the surface and (iv) rainfall intensity (AWS) of at least $10\text{mm}\cdot\text{h}^{-1}$ (Klaassen, 1988) (Fig. 1c,d). The convective nuclei were identified using GOES-16 imagery, determined as a contiguous area of at least 40 pixels with BT lower than 235K ($\leq -38^\circ\text{C}$) over Rio Claro station, according to previous studies (Ribeiro et al., 2019).

2.5 Definition of day-night differences in convective rainfall

3 Results and Discussion

205 A complete database comprising the results of high-frequency sampling of convective rainfall events occurring during the study period at the Rio Claro site (isotope characteristics of rainfall as well as selected meteorological parameters characterizing these events) can be found et: (dos Santos et al., 2023). Table 1 contains median values of isotope and meteorological parameters for the studied rainfall events, separated into night-time and day-time categories.

210 The rainfall samples collected in this study generally do not represent consecutive pairs of day-night data during the same day. Daytime data are related to rainfall samples collected in Rio Claro station from 07:00 to 18:59 local time (10:00-21:59 UTC) whereas night-time data represent the period 19:00-06:59 local time (22:00-09:59 UTC). Therefore, the labelling of convective rainfall samples as 'day' or 'night' is directly related to the period of their collection at the Rio Claro station. It was not the focus of this study to evaluate the formation of convection processes and evolution of a convective system, because we only collected rainfall samples in a single point. An evaluation of the evolution of convection during the day-night using high-frequency strategies would require a range of collection stations capable of capturing the formation of the convective system and its spatial and temporal evolution. Although, in the tropics, a substantial part of the convection systems is developed during the day (Warner et al., 2003; Romatschke and Houze, 2010), they can generate rain events in the afternoon and at night, not

Formatado: Fonte: Não Negrito

occurring in the same place. Proper sampling of these systems, following their formation, development, and decay would require a complex and expensive sampling strategy.

2.6 Statistical tests

The Shapiro-Wilk test was applied to verify that the data distribution was normal (parametric) or non-normal (non-parametric) (Shapiro and Wilk, 1965). A significant difference (p -value < 0.05) indicates a non-parametric distribution. A Spearman rank correlation test was used for nonparametric data distribution, whereas Pearson's linear correlation test was applied for parametric data. A Kruskal-Wallis nonparametric test (Kruskal and Wallis, 1952) was applied to test statistical differences (p -value < 0.05) between the isotopic compositions ($\delta^{18}\text{O}$ and d -excess) for day-night during summer, and between autumn and spring. All tests were performed with significance levels defined by a p -value (p) < 0.05 , using R statistical package (R Core Team, 2022).

3 Results

3.1 Seasonal variations of rainfall isotopes and meteorological parameters

The high-frequency sampling allowed a more detailed and robust analysis of rainfall formation processes and its isotope characteristics as compared to previous studies in the region (dos Santos et al., 2022; Dos Santos et al., 2019), which were based on monthly or daily composite rainfall samples. Figure 2a illustrate this monthly perspective of isotope characteristics ($\delta^{18}\text{O}$ and d -excess) of rainfall for the study period (September 2019 – February 2021) at the Rio Claro site. It reveals a sharp seasonal isotopic contrast between rainy and dry season (austral summer and winter, respectively). The Local Meteoric Water Lines (LMWL) for the Rio Claro site based on monthly cumulative and high-frequency samples (Fig. A1 – Appendix A) cannot be directly compared because of not complete coverage of rainfall in the given month by the high-frequency sampling, and selected meteorological parameters of monthly rainfall. The high-frequency sampling strategy employed in the study was aimed to capture specific rainfall events for each season (cf. Fig. 2a).

Seasonal variations of the isotopic composition of monthly cumulative precipitation and selected meteorological parameters (latent heat flux, outgoing longwave radiation flux (OLR), monthly amount of rainfall) recorded at the Rio Claro site during the study period (September 2019 – February 2021), are presented in Fig. 2. The monthly values of meteorological parameters were split in Fig. 2 into day and night fraction. Superimposed on monthly values of $\delta^{18}\text{O}$ presented in Fig. 2a are monthly averages of this parameter derived from high-frequency sampling of the convective events. Although they do not cover uniformly the presented study period, it is clear that they follow the seasonal variations of $\delta^{18}\text{O}$ derived for monthly cumulative precipitation samples. A sharp seasonal contrast in the isotopic composition of rainfall for rainy and dry season (austral summer and winter, respectively) is apparent in Fig. 2a. The Local Meteoric Water Lines (LMWL) for the Rio Claro site based on monthly cumulative and high-frequency samples (Fig. 3) cannot be directly compared because of incomplete coverage of

Formatado: Fonte: Não Negrito

Formatado: Título 1

rainfall in the given month by the high-frequency sampling. The high-frequency sampling strategy employed in the study was aimed to capture specific rainfall events for each season (cf. Fig. 2a).

The seasonal and day-night distributions/fluctuations of convective activity characterized by latent heat flux and OLR flux (Fig. 2b,c) and rainfall amount (Fig. 2d) were observed during the study period, resulting in different conditions for occurrence of convective events and high-frequency sampling of rainfall. In austral winter, a season characterized by dry conditions in the south-central tropics of Brazil, convective rainfall events were largely absent (Fig. 2a). No rainfall was collected at night during spring (convective events occurred predominantly during day hours). Covid-19 restrictions precluded rainfall collection at night. Contrary to summer months, during autumn, spring and winter/spring, latent heat fluxes were lower (Fig. 2b) and outgoing longwave radiation/OLR was larger/higher (Fig. 2c), which in turn may have inhibited convective development related to thermal forcings (Houze, 1997, 1989). During summer, strong diurnal heating and persisting convective activity resulted in nearly equal total rainfall amounts during day (51%) and night (49%) (Fig. 2d).

3.2 Day-night differences in Intra-event variability of the isotope and meteorological parameters and isotopic

Temporal evolution of isotope characteristics of convective rainfall ($\delta^{18}\text{O}$, d -excess) and selected meteorological parameters (brightness temperature, MRR reflectivity and rainfall amount) of convective rainfall events sampled and analyzed in this study is presented in Fig. 4.

Strong day-night variations in the isotopic parameters $\delta^{18}\text{O}$, d -excess of convective rainfall were observed during the austral summer (red-box-plots in Fig. 3). Day and night median $\delta^{18}\text{O}$ values were equal -7.5‰ and -13.0‰ , respectively. During daytime, higher $\delta^{18}\text{O}$ values (-4.4‰ – -11.6‰ , Fig. 3a), lower d -excess values (1.2‰ – 18.4‰ , median 8.4‰ –Fig. 3d), lower AWS rain rates (median $1.0\text{mm}\cdot 5\text{min}^{-1}$ –Fig. 3g) and AWS rainfall amount (median 16.9mm) were observed. In contrast, lower $\delta^{18}\text{O}$ values (-7.9‰ – -15.2‰), higher d -excess (4.8‰ – 21.4‰ , median 16.7‰), higher AWS rain rates (median $1.8\text{mm}\cdot 5\text{min}^{-1}$) and AWS rainfall amount (median 26.9mm) were observed night-time convective events. The non-parametric Kruskal-Wallis test shows significant differences between day and night isotopic composition ($p < 0.0001$ for $\delta^{18}\text{O}$ and d -excess).

Similar $\delta^{18}\text{O}$ values (Fig. 3b,c) were observed in autumn (median -3.1‰) and spring (median -3.2‰), while d -excess values (Fig. 3e,f) and AWS rain rates (Fig. 3h,i) differ between both seasons, (autumn: 16.8‰ and $0.6\text{mm}\cdot 5\text{min}^{-1}$; spring: 22.2‰ and $1.2\text{mm}\cdot 5\text{min}^{-1}$) (Fig. 3e,f). The Kruskal-Wallis test shows significant differences between autumn and spring and for the d -excess ($p=0.0039$) and AWS rain rates ($p=0.04$), except $\delta^{18}\text{O}$ ($p=0.36$).

Differences in convective rainfall between seasons were also observed in the origin of moisture tracked back by HYSPLIT modelling (Fig. 1e), accompanied by differences in median $\delta^{18}\text{O}$ and d -excess values (in parentheses below, respectively) (Fig. 3-color coded). In summer, convective events during daytime exhibited trajectories from Amazon (-10.4‰ and 13.4‰) and Southwest (-6.7‰ and -7.1‰), and predominantly from Amazon at night-time (-13.0‰ and -16.7‰). The Atlantic Ocean

Formatado: Fonte: Negrito

Formatado: Com marcadores

Formatado: Inglês (Estados Unidos)

moisture source was dominant during autumn (3.3‰ and 17.2‰ for daytime, -2.8‰ and 16.2‰, night time) and spring (-3.1‰ and 22.9‰), but also mixing with more isotopically-depleted moisture of the Amazon origin (-4.1‰ and 19.7‰) was suggested by HYSPLIT simulations for few events.

Figure 4 illustrates different meteorological scenarios for isotope parameters ($\delta^{18}\text{O}$ and d excess). During summer, in daytime higher $\delta^{18}\text{O}$ and lower d excess values correspond to low relative humidity values (RH) (Fig. 4a), high lifting condensation level (LCL) (Fig. 4f) and low brightness temperature (BT) (Fig. 4k). At night time, slightly lower $\delta^{18}\text{O}$ values and higher d excess correspond to higher RH (Fig. 4b), lower LCL (Fig. 4g) and higher BT values (Fig. 4l). For these variables strong and significant ($p < 0.05$) correlations were observed (Table 1): during daytime $\delta^{18}\text{O}$ -RH ($r = -0.51$), $\delta^{18}\text{O}$ -T ($r = -0.64$), $\delta^{18}\text{O}$ -AWS rain rate ($r = -0.57$), d excess and AWS rain rate ($r = 0.61$), d excess and Z ($r = 0.61$), d excess and MRR rain rate ($r = 0.61$) and night time $\delta^{18}\text{O}$ -RH ($r = -0.74$), d excess and RH ($r = 0.51$), $\delta^{18}\text{O}$ -LCL ($r = 0.75$), d excess and LCL ($r = -0.52$), $\delta^{18}\text{O}$ -T ($r = 0.50$).

During autumn and spring, the isotopic composition of convective rainfall is influenced by frontal systems (Fig. 4r,s,t) (Dos Santos et al., 2019) which are characterized by (i) the passage of a cold front over the study area, (ii) instability (frontal), when a cold front is localized in the south of Brazil and it generates changes in the regional atmosphere over São Paulo, and (iii) when the cold front is localized in the Atlantic Ocean near Southeast portion of Brazil and interacts with regional atmosphere, generating a low pressure (frontal). In summer, frontal systems and frontal instabilities occurred during the daytime (Fig. 4p), while instability (thermal) and low pressure were present only at night (Fig. 4q). The instability (thermal) is the atmospheric ascend related to surface heat in inland Brazil, mainly during summer.

Slightly higher median meteorological values were observed in spring when compared to autumn, except for LCL (449m autumn night and 225m spring), RH (AWS, 95% autumn day and 93% spring) and RH (HYSPLIT, 78% autumn day, 73 autumn night and 41% spring) (Table B1). Also, the relations between rainfall isotopic composition and meteorological parameters are not very clear in these seasons (Fig. 3). In general, correlations between isotope ratios and meteorological variables in spring and in autumn are rather weak (Table 1), except for $\delta^{18}\text{O}$ -BT during autumn ($r = 0.53$).

3.3 Conceptual model of convective rainfall during summer

A conceptual model of the observed day/night isotopic variability of convective rainfall at the Rio Claro site is presented in Fig. 5. The measured meteorological variables help us to better characterize the convective cloud/rainfall during passage over the sampling site, the local atmosphere surface conditions, and their impact on the observed isotope signatures of rainfall. BT and LCL are related to the convective cloud depth (Machado and Laurent, 2004; Ribeiro et al., 2019) and cloud base (Risi et al., 2019; Hu et al., 2022), respectively. RH and rainfall rates (from MRR and from AWS) indicate atmospheric conditions below the cloud base and at the surface (Graf et al., 2019; Aemisegger et al., 2015a).

310 For daytime conditions, median values of meteorological and isotope parameters suggest strong convective cloud depth and elevated cloud base (lower BT and high LCL values), the later resulting in longer interaction time between raindrops the ambient atmosphere below the cloud base level. Lower RH enhances partial evaporation of raindrops, decreasing median value of rainfall rate (both MRR and AWS readings), and producing less negative $\delta^{18}\text{O}$ and lower d -excess values. During night-time, less vigorous convective cloud depth (higher BT) and low cloud base level (low LCL) were observed, which resulted in reduced time of interaction raindrops with the atmosphere below the cloud base. High RH at the surface combined with higher median rainfall intensity, further reduced the extend of raindrops evaporation. Consequently, stable isotope signatures generated during in-cloud processes were transferred without substantial changes to the samples of rainfall collected at the ground.

4 Discussion

320 We are not directly interpreting the convection processes (not include vapor isotopes data), but rather the consequence of this mechanism reflected in rainwater. For this reason, our dataset represents case studies of rain events over our collection point (Fig. 1), whose classification was based mainly on point vertical radar observation, agreed with Houze (1997), that the convective adjective must be used to describe the precipitation (or radar echo) and convection (or convective activity) is a dynamic concept, the rapid, efficient, vigorous overturning of the atmosphere, directly related to the formation of clouds in the tropics (Houze, 1997, 1993).

325 Isotopic composition of convective rainfall is a function of two main factors: (i) rainout history of moist air masses during their transport in the atmosphere, from the source region(s) to the collection site, and (ii) local effects associated with convective cloud characteristics at a given location linked to the fractionation steps associated with in-cloud phase changes of water such as vapour to liquid and/or, vapour to solid, and modifications of rainfall isotopic composition below the cloud-base level due to partial evaporation of raindrops as well as isotope exchange with the ambient moisture.

330 Regional aspects of atmospheric moisture transport to the Rio Claro site are illustrated in Fig. 1e showing representative HYSPLIT backward trajectories associated with convective rainfall whereas maps of vertically integrated moisture flux in the region are shown in Fig. 6. During summer, most of the moisture supply to the rainfall collection site is associated with northwest-southeast winds bringing moisture from the Amazon basin. Moist air masses of Atlantic origin are transported westward over the Amazon Forest, undergoing intensive recycling and rainout. Strong topographic blocking effect of the Andes induces a change in the wind direction to northwest-southeast, along the eastern slope of the Andes, allowing flow of moisture from the Amazon Basin to the southeast of Brazil (Fig. 6a) (Marengo et al., 2004; Vera et al., 2006). Along this pathway, the occurrence of regional convective activity (Fig. 6d) generates successive convective systems resulting in continuous rainout (Fig. A2) and vapour recycling (Moerman et al., 2013; Risi et al., 2008; Vimeux et al., 2011), which leads to the characteristic depletion of convective rainfall in heavy isotope contents ($\delta^{18}\text{O}$ around -10%). Intensive convective activity during summer results in large amounts of rainfall reaching the land surface during this season (Fig. A2).

In contrast to summer rainy season when moist, rain-producing air masses arriving at Rio Claro station are predominantly of the Amazon origin, during autumn and spring the rainfall is associated exclusively with Atlantic Ocean and/or Amazon, respectively. These air masses and largely suppressed convective activity during autumn (Fig. 6e) and spring (Fig. 6f) generate convective systems with lower continuous rainout (Fig. A2) and vapor recycling. Very high $\delta^{18}\text{O}$ values, with median equal 3.1‰ (autumn) and 3.2‰ (spring), accompanied by high d -excess values (median equal ca. 16.8 and 22.2‰, respectively (cf. Fig. 2), can be explained only by two processes: (i) first step condensation of water vapour of marine origin (Atlantic Ocean), and/or (ii) first step condensation of evapotranspired moisture of continental origin which has the isotopic composition of regional rainfall in the study area, stored in the soil during the rainy season ($\delta^{18}\text{O}$ equal ca. 10 per mil). HYSPLIT modelling suggests further that, during spring, two types of moist air masses are contributing to the characterize differences in isotopic composition of convective rainfall: (i) continental air masses arriving from the Amazon, and (ii) maritime air masses arriving from the Atlantic Ocean. It is apparent from Fig. 3b,c that these two types of air masses reveal slightly different isotope signatures: median $\delta^{18}\text{O}$ correspond to 4.1‰ and 3.1‰, respectively, with d -excess values substantially lower for continental moist air masses when compared to maritime air masses (19.7‰ and 22.9‰, respectively) (Fig. 3e,f). It is apparent from Fig. 1e, that backward trajectories starting at the Atlantic Ocean may interact also with the continent (mixing with re-evaporated water vapour and partial rainout over the continent) before they reach the Rio Claro site. This is supported by slightly reduced $\delta^{18}\text{O}$ and elevated d -excess values observed when compared to rainfall events of purely continental origin.

The high frequency of rainfall sampling implemented in this study revealed yet another dimension of the isotopic variability of summer rainfall in the tropics: day versus night time differences in convective rainfall (cf. Fig. 3a,d). The night time rainfall is depleted in heavy isotopes and has elevated d -excess values, when compared to the daytime rainfall. During summer rainy season in the southwest of Brazil is under overwhelming influence of moist air masses arriving from the Amazon basin. Night time rainfall events were predominantly from Amazon air masses. The occurrence of night time events was limited and likely linked to the occurrence of the low level jet during the night (Saulo et al., 2000; Nicolini et al., 2002). These air masses have a long history which could be linked to long residence time of water vapor in the atmosphere, in the order of 10 days (Gimeno et al., 2010). This in turn, combined with rainout and moisture recycling, may lead to distinct depletion in heavy isotope contents and elevated d -excess values of the moisture precipitating over the Rio Claro site. Therefore, it is highly unlikely that the sharp day-night contrast in the isotope characteristics of convective rainfall shown in Fig. 3a,d is generated by only moist air masses of different origin. Instead, we suggest that those strong diurnal variations of the isotopic composition of convective rainfall in the inland tropics of Brazil are mainly controlled by local effects.

Impact of local processes on the isotopic composition of convective rainfall in the tropics is illustrated by the conceptual model presented in Fig. 5. This diagram combines (a) meteorological parameters characterizing the convective cloud structure (cloud-top temperature and cloud-base level) and rainfall interactions with the local atmosphere below the cloud-base level (ground-level relative humidity, lifting condensation level, raindrops dimensions and rainfall rate) with (b) the processes

375 ~~modifying the isotopic composition of raindrops below the cloud-base level (partial evaporation and isotope exchange with~~
~~ambient moisture). We suggest that night-time isotopic composition of convective rainfall largely reflects regional conditions~~
380 ~~characterized by presence of moist air masses of Amazon origin depleted in heavy isotopes and having elevated d -excess~~
~~values, with the LLJ playing a relevant role in the moisture transport from the Amazon to the collection-site area. It is suggested~~
~~that partial evaporation and isotope exchange of raindrops below the cloud-base level seems to be suppressed at night due to~~
~~number of factors such as: (i) shorter travel time of raindrops to the ground due to both lower cloud-base level and higher~~
385 ~~terminal velocity of large raindrops formed during night-time events, (ii) smaller relative mass reduction of large raindrops~~
~~leading to smaller modification of their isotopic composition due to partial evaporation, (iii) higher RH of the ambient~~
~~atmosphere below the cloud-base level reducing intensity of raindrops evaporation. These factors change during daytime,~~
~~resulting in a substantial modification of the original isotopic composition of raindrops leaving the cloud base (longer travel~~
~~time of raindrops, higher relative mass reduction of raindrops, lower RH of ambient atmosphere below the cloud-base level).~~
385 ~~Our conceptual model supports previous studies related to possible factors modifying the isotopic composition of precipitation~~
~~below the cloud base level such as drop-size distribution (Muller et al., 2015; Managave et al., 2016), below-cloud RH (Lee~~
~~and Fung, 2008), height of the cloud base (Wang et al., 2016) and rain intensity (Graf et al., 2019). However, it is mentioned~~
~~that a more detailed assessment of precipitation evaporation below the cloud base must be conducted and include further details~~
~~of the vertical profiles of temperature and humidity as well as water-vapor isotopes information if possible.~~

390 ~~Absence of day-night isotope contrasts of rainfall during the autumn and spring seasons (cf. Fig. 2) is probably related to~~
~~lower surface heating and hence lower possibility of convection to generate convective rainfall by thermal conditions (cf. Fig.~~
~~6e,f). Apparently, generally weaker convection activity of the regional atmosphere during this period does not generate day-~~
~~night differences in the extent and intensity of rain-producing convective systems, large enough to induce discernible~~
~~difference in the isotopic characteristics of rainfall.~~

395 ~~In this figure, radar ecos for all sampled events. The emphasizes the absence of pattern in measured values for the~~
~~reflectivity (Z_c) on the vertical profile (Fig. 4a-b, g-h, m-n, s-t), only near surface higher values were observed (from 2km to~~
~~200m), indicating an increase in raindrop size, hence an increase in Z values and rain rates. Despite the similar vertical~~
~~structure, the temporal evolution was quite distinct between the events, according to the season when the event was collected.~~
~~The brightness temperature of GOES-16 (BT) has distinct temporal distributions between events (Fig. 4e-f, k-l, q-r, w-x),~~
400 ~~despite the no relationship observed between variations of BT and a change in isotope values.~~

~~For the events collected during the summer, 2020/02/01-day (Fig. 4c,e) and 2020/01/30-night (Fig. 4d,f) the duration were~~
~~similar (20min and 25min, respectively), similar temporal $\delta^{18}\text{O}$ evolution (-10.29 ~ -10.07‰ (stationary trend) and -10.13 ~ -~~
~~9.91‰ (little increasing trend) and similar rain rates trends (2.8 ~ 0.1mm and 4.4 ~ 0.1mm), respectively. Contrary to the~~
~~2021/02/24-day (Fig. 4i, k) and 2020/02/10-night (Fig. 4j, l) events, that had similar longer duration (02h01min and 02h39min,~~
405 ~~respectively), however, had distinct variations of $\delta^{18}\text{O}$ and rain rates (-7.60 ~ -4.47‰ (increasing trend) and -12.35 ~ -13.99‰~~
~~(decreasing trend) and 2.6 ~ 0.3mm and 0.6 ~ 0.6mm, respectively), illustrate the remarkably difference between day (enriched)~~
~~and night (depleted) isotopic composition. Lower d -excess values were observed on 2021/02/24 (9.3 ~ 1.2‰) 2020/02/01 (11.3~~

410 ~7.0‰) and 2020/02/10 (21.4 ~ 4.8‰). While for 2020/02/01 and 2020/02/10 these lower *d*-excess values have been observed at the end of event, when rain rates were lower (0.01mm and 0.8mm, respectively), indicating the residual precipitation, as the rainfall dissipates (Celle-Jeanton et al., 2004), on 2021/02/24 lower *d*-excess values were observed in some parts of the event, associated to lower Z values (from 16:38 to 17:15). The differences on isotopic composition and a possible effect to below-cloud evaporations for these events are detailed discussed in section 3.4.

415 For the events collected during the autumn (2020/06/09 (Fig. 4o) and 2020/05/23 (Fig. 4p) values and variations on $\delta^{18}\text{O}$ were similar (-3.67 ~ -2.76‰ and -2.67 ~ -2.75‰), the first event showed a little decreasing trend, while the second is stationary. On the other hand, 2020/06/09 and 2020/05/23 *d*-excess values (25.4 ~ 6.3‰ and 16.7 ~ 19.0‰, respectively), trends (w-shaped and stationary), RR (6.2 ~ 0.01mm and 2.6 ~ 0.2mm), BT (-55 ~ -35°C and -60 ~ -52°C) and vertical structure variable (two peaks of higher Z values near-surface (4m) and one peak oh high Z values at start (Fig. 4n), respectively. Despite the decrease of BT values along the time observed in the 09/06/2020 event, lower *d*-excess values and a slight $\delta^{18}\text{O}$ increase have been observed during the peak of RR. These changes on isotope distribution could be related to the passage of convective development zones during the event evolution (Risi et al., 2010), from a strong convective activity, corroborated by lower BT values (-55 ~ -52°C) and higher Z (between 17:04 and 14:44), to convection transition activity, represented by an increase on BT (-51 ~ -48°C) and lower Z (between 17:46 to 18:09) and finally, to lower convective development, characterized by higher BT values (>-45°C), and higher Z (between 18:12 to the end).

425 Spring convective events, collected on 2019/11/05 (Fig. 4u,) and 2020/11/18 (Fig. 4v), have shown opposite isotope variations (-3.00 ~ -1.78‰ and -2.76 ~ -5.40‰) and trends (increasing and decreasing, respectively). Values of RR, normally higher, BT, normally lower, did not present relationship with the isotopic variation (Fig. 4w, x). Values of *d*-excess were stationary on 2019/11/05 event (28.0 ~ 21.0‰), while presented an increase trend during the event collected on 2020/11/18 (10.2 ~ 23.1‰). Any value of *d*-excess were lower than 10‰. The vertical profile of Z is quite distinct between spring events (Fig. 4s, t), higher Z values near-surface was observed at the start and lower at the end of 2019/11/05, while on 2020/11/18 a strong peak of Z occurred at the end (between 16:15 and 16:25). These temporal evolutions in the vertical profile of events 2019/11/05 and 2020/11/18 illustrate the opposite isotope trends (increasing and decreasing, respectively) generally related to the fast condensation and rainfall formation due to the strong updrafts (e.g. Sodemann, 2006; Gedzelman and Lawrence, 1990) and isotopic equilibrium between droplets and vapor (e. g. Celle-Jeanton et al., 2004; Barras and Simmonds, 2009; Muller et al., 2015), respectively.

430 The weather systems (indicated for each rainfall event in Fig. 6) interacting with the moisture available producing the rainfall systems. A large influence of the cold fronts was observed before, during and after their passage over the study area. Convective rainfall directly formed by the frontal systems (cold front acting at the study area) for 2019/11/05, 2020/11/18, 2020/05/23 and 2020/02/01 events had distinct isotope trends (increasing, decreasing, stationary and stationary), respectively. The instability (frontal) system (when a cold front is localized in the south of Brazil and generates changes in the regional atmosphere over São Paulo state) occurred for 2020/06/09 (decreasing) and 2021/02/24 (increasing trend) events, while thermal instability formed by atmospheric ascend due to surface heat in inland Brazil of 2020/01/30 (little increasing trend).

and low pressure (frontal) system (when the cold front is localized in the Atlantic Ocean near Southeast portion of Brazil and interacts with regional atmosphere) for 2020/02/10 (decreasing trend).

The large diversity of trends is quite different observed in previous studies of cold fronts in mid-latitudes, generally related to the V-shaped and strong δ depletion (e. g. Aemisegger et al., 2015; Gedzelman and Lawrence, 1990; Celle-Jeanton et al., 2004; Muller et al., 2015). Apparently, for intra-events presented here, it is difficult to relate the contribution of weather systems control of isotopic variability, due to the different conditions of temperature, moisture available and convective activity (lower during autumn-spring and higher during summer in Fig. 2) along the seasons. Perhaps, which contributes to connecting regional processes to isotope variations, mainly the large d -excess distributions, is the associate origin and transport with inter-event evaluation, illustrated in Fig. 5 and 6 detailed in the 3.3. section.

3.3. Inter-event variability of the isotope and meteorological parameters

Figure 5 shows Hysplit ensemble trajectories calculated for each analyzed rainfall event, divided into seasons (summer, autumn and spring). It is clear from Table 1 and Fig. 5 that three summer events, undoubtedly associated with moist air masses arriving from the Amazon basin (2020/02/10, 2020/02/01 and 2020/01/30), have remarkably similar isotope and meteorological characteristics ($\delta^2\text{H}$, $\delta^{18}\text{O}$, d -excess, RH), irrespectively whether they are day-time or night-time events. In contrast, the day-time event which occurred on 2021/02/24 and revealed higher δ values, lower d -excess and lower relative humidity, was fed by moisture of Atlantic origin (Fig. 5a).

The estimated vertical integral eastward vapor fluxes using data from ERA-5 (Fig. 6) combined with Hysplit air masses backward trajectories, shows clearly the predominant influence of Amazon moisture for 2020/02/01, 2020/01/30 and 2020/02/10 convective events, representing summer events (Fig. 6a, b, d), marked by the negative values for vertical vapor fluxes ($< -250 \text{ kg m}^{-1} \text{ s}^{-1}$) over the Amazon basin (indicating the direction of moisture vapor flux from the Ocean to Amazon Forest) and positive values ($> \sim 500 \text{ kg m}^{-1} \text{ s}^{-1}$) over the central-southern portion of Brazil (indicating the direction of vapor flux from Amazon basin with pathways over the study area to the Atlantic Ocean). The higher positive values ($\sim 750 \text{ kg m}^{-1} \text{ s}^{-1}$ in red color in Figure 6a, b, d) illustrate the acts of cold fronts between the continental portion and the Atlantic Ocean. This regional pattern was not observed during on 2021/02/24, eastward vapor flux is positive and has high values over the Atlantic Ocean ($250 \sim 750 \text{ kg m}^{-1} \text{ s}^{-1}$), corroborating the distinct moisture transport, δ values and relative humidity values.

The two events representing autumn season (2020/05/23 - night-time event and 2020/06/09 – day-time event) were associated with mean trajectories similar to those calculated for the spring season (Fig. 5b). In this case the continental origin of moist air masses (south-western Brazil) is more pronounced (2020/05/23), whereas the Amazon-type trajectory starts in southern Atlantic and does not reach the boundary of the rainforest. In fig. 6, the eastward vapor flux illustrates the continental origin of moist air masses on 2020/05/23 and Atlantic origin for the 2020/06/09. While on 2020/05/23 negative values ($-500 \sim -250 \text{ kg m}^{-1} \text{ s}^{-1}$) were observed in south-western Brazil (indicating transport from the Atlantic Ocean to the continent), which formed a vapor flux of positive values ($500 \sim 750 \text{ kg m}^{-1} \text{ s}^{-1}$) from western Brazil to the study area (Figure 6f), on 2020/06/09

475 slight negative values ($-250 \sim 0 \text{ kg m}^{-1} \text{ s}^{-1}$) of eastward vapor flux over Amazon basin indicate the decrease of rainforest
moisture flux, positive vapor flux values ($250 \sim 500 \text{ kg m}^{-1} \text{ s}^{-1}$) over the western portion of continental Brazil and study area
corroborate that the trajectory started from Atlantic Ocean to arrive directly over the Rio Claro station (Fig. 5b and Fig. 6e).

480 Finally, two day-time events available for the spring season (Fig. 5c) also reveal contrasting origin of moisture. The mean
trajectory for the 2020/11/18 belongs clearly to the Amazon category, although it is passing only over the south-eastern
boundary of the Amazon rainforest and has much shorter extension when compared with the Amazon trajectories observed
during the summer season, thus positive values of eastward vapor flux ($250 \sim 750 \text{ kg m}^{-1} \text{ s}^{-1}$) are not distribution along from
Amazon basin to Atlantic Ocean as typically observed previously (Fig. 6h). The mean trajectory for the second event
(2019/11/05) and higher positive eastward vapor flux ($> 500 \text{ kg m}^{-1} \text{ s}^{-1}$, Fig. 6g) are circling around the Rio Claro, pointing to
the continental origin (southern Brazil) of moist air masses responsible for this event.

485 It is apparent from Fig. 5a and Table 1 that three summer events mentioned above (2020/02/10, 2020/02/01 and 2020/01/30)
are very consistent in terms of the length and shape of backward trajectories of moist air masses, as well as isotope
characteristics of the rainfall events produced from those air masses. The mean $\delta^2\text{H}$, $\delta^{18}\text{O}$ and d -excess values for those three
events are equal -76.6 , -11.4 , 15.5% , respectively. The ground-level relative humidity is also consistent (mean value 94% ,
range ca. 5%). Autumn and spring events also reveal remarkable degree of consistency in terms of origin of moisture and
isotope characteristics of rainfall (cf. Table 1 and Fig. 5b,c). The mean $\delta^2\text{H}$, $\delta^{18}\text{O}$ and d -excess values are equal -6.4 , -3.4 ,
 19.1% , respectively. Mean relative humidity is equal 90.8% . Those dramatic differences between δ values of convective
rainfall sampled during summer months and that sampled during spring and autumn (ca. 8% for $\delta^{18}\text{O}$ and 70% for $\delta^2\text{H}$),
generated under similar thermal conditions in the region, call for explanation. Also, substantially higher mean d -excess value
for spring and autumn events (the difference with respect to summer mean value equal 3.6%) needs to be understood.

490 We suggest that isotope characteristics of convective events investigated in this study (both the δ values and the d -excess)
are controlled by three major factors: (i) the origin of moisture and the degree of rainout of moist air masses responsible for
precipitation over the Rio Claro site, (ii) the backward flux of water vapor released by the continent to the regional atmosphere,
and (iii) possible modification of isotopic signatures of rainfall due to partial evaporation of raindrops and their interaction
with ambient water vapor reservoir below the cloud base.

500 The overwhelming majority of moist air masses arriving at Rio Claro during summer have their source somewhere in the
equatorial Atlantic and are subject to long rainout history extending over several thousand kilometers. Along this pathway
those air masses interact with the Amazon rainforest. Intensive recycling of moisture leads to small continental gradient of δ
values of rainfall across the Amazon basin (Salati et al., 1979; Rozanski et al., 1993) and elevated d -excess (Gat, J. R., &
Matsui, 1991). While arriving at Rio Claro, those air masses are strongly depleted in heavy isotopes due to enhanced rainout
over the second portion of their trajectory (after deflection of moist air masses from the Andes), but they maintain the elevated
deuterium excess inherited through interaction of maritime moisture with the Amazon rainforest. Such air masses generate
precipitation depleted in heavy isotopes, with high d -excess value, as observed over Rio Claro.

510 The analyzed convective events representing spring and autumn season have substantially shorter 10-day trajectories suggesting that atmospheric “pump” transporting moisture from the equatorial Atlantic to the Amazon basin is much weaker or non-existing during this time of a year. Those short trajectories also suggest enhanced interaction with the surface of the continent. The backward flux of moisture from the surface to the atmosphere, generated in evapotranspiration processes apparently becomes the major source of moisture for rainfall occurring during spring and autumn in the region.

515 It is a generally accepted fact that transpiration process, at its steady state, is a non-fractionating process i.e. it returns the soil water pumped by the plants to the atmosphere without any discernible change of its isotopic composition (e. g. Cuntz et al., 2007; Flanagan et al., 1991; Dongmann and Nürnberg, 1974). In the study region we have distinct dry and wet period (cf. Fig.2d). If we assume that soil water accessible to plants has the isotopic characteristics equal to mean values of the four summer events discussed above (-68.67, -10.28, 13.5‰, for $\delta^2\text{H}$, $\delta^{18}\text{O}$ and d -excess, respectively), than water vapour released to the regional atmosphere in the transpiration process will have the same isotopic signatures. Now, if we assume that this water vapour is lifted up by convection processes and reaches the condensation level, the isotopic composition of the first condensate can be easily calculated assuming isotope equilibrium between gaseous and liquid phase of water at the cloud:

520
$$\delta_L = \alpha_{eq}(1000 + \delta_V) - 1000 \quad (1)$$

525 where δ_L and δ_V signify delta values of liquid (condensate) and vapor phase, respectively, at isotopic equilibrium, whereas α_{eq} stands for equilibrium fractionation factor. Equilibrium fractionation factors for ^2H and ^{18}O were calculated using empirical expressions proposed by (Horita and Wesolowski, 1994). The assumed condensation temperature was equal 18°C (cf. Tdw for spring and autumn events – Table 1). The calculated isotope characteristics of the first condensate are equal +12.2, -0.46 and 15.8‰, for $\delta^2\text{H}$, $\delta^{18}\text{O}$ and d -excess, respectively. Large potential of the transpiration process in generation of isotopically enriched rainfall is clearly seen from the above exemplary calculation.

530 In addition to water vapor generated in the transpiration process, the backward vapor flux from the continent to the regional atmosphere will also include evaporation of surface water bodies located in the footprint area of the rainfall collection site. Evaporation of surface water bodies will generate vapor slightly depleted in heavy isotopes when compared to the source water subject to evaporation, and isotopic composition of this vapor will be located on the Local Evaporation Line (LEL), to the left-hand side of the Local Meteoric Water Line, thus exhibiting high d -excess values (e. g. Rozanski et al., 2001). The fact that the mean d -excess value of spring and autumn convective rainfall events analyzed in this study (ca. 19.1‰) is higher than that obtained for the mean isotopic composition of four analyzed summer events (ca. 13.5‰ - cf. discussion above) provides the evidence that the flux of water vapor to the regional atmosphere, a part of dominating contribution generated by the transpiration process (10-day mean evapotranspiration values of summer, spring and autumn events are equal 41mm, 31mm and 24mm, respectively), will also contain the fraction originating from surface water evaporation in the region.

3.4. Assessing the impact of below-cloud processes on the isotope characteristics of convective precipitation

The third factor which may contribute to the observed large differences between δ values of convective rainfall events sampled during summer months and those collected during spring and autumn, (ca. 8‰ for $\delta^{18}\text{O}$ and 70‰ for $\delta^2\text{H}$), generated under similar thermal conditions in the region, is the possible modification of the isotopic signatures of raindrops due to their partial evaporation and interaction with ambient water vapor reservoir below the cloud base level. This issue will be discussed below in some detail. As the isotopic composition of near-ground water vapour during the sampled rainfall events has not been measured, application of the interpreting framework for below-cloud effects on the isotopic characteristics of rainfall proposed by Graf et al. (2019) cannot be adopted here. Instead, a rough, semi-quantitative assessment of the impact of those effects in the context of the discussed isotope data will be presented below. The assessment will focus on two rainfall events sampled in summer: (i) 2020/02/10 night-time event, and (ii) 24/02/2021 day-time event.

Due to lack of appropriate data, a number of simplifying assumptions has to be made: (i) median values of isotope and meteorological parameters recorded for each analysed event (Table 1) will be used in the calculations, (ii) linear interpolation of air temperature and relative humidity between the cloud base level and the ground level will be adopted, (iii) it will be assumed that atmosphere is saturated with water vapour at the cloud base level (RH = 100%), and (iv) the reservoir of water vapour below the cloud base level is isotopically homogeneous.

Isotopic evolution of raindrops falling through unsaturated humid atmosphere beneath the cloud base level will be calculated using generally accepted conceptual framework for isotope effects accompanying evaporation of water into a humid atmosphere (Craig and Gordon, 1965; Horita et al., 2008). Isotopic evolution of an isolated water body (e.g. falling raindrop) evaporating into a humid atmosphere can be described by the following equation (Gonfiantini, 1986):

$$\delta = \left(\delta_o - \frac{A}{B} \right) F^B + \frac{A}{B} \quad (2)$$

where

$$A = \frac{h_N \delta_A + \varepsilon_{kin} + \varepsilon_{eq} / \alpha_{eq}}{1 - h_N + \varepsilon_{kin}} \quad (3)$$

and

$$B = \frac{h_N - \varepsilon_{kin} - \varepsilon_{eq} / \alpha_{eq}}{1 - h_N + \varepsilon_{kin}} \quad (4)$$

Parameter F signify the remaining fraction of the evaporating mass of water (raindrop) while δ_A stands for the isotopic composition of ambient moisture. Initial and actual isotopic compositions of the evaporating water body, expressed in δ notation, are represented by δ_o and δ , respectively (expressed here as a fractions of unity). The meaning of the remaining parameters in equations (3) and (4) reads as follows:

h_N – relative humidity of ambient atmosphere, normalized to the temperature of the evaporating water body

α_{eq} – temperature-dependent equilibrium fractionation factors, derived from empirical equations proposed by Horita and Wesolowski (1994).

ε_{eq} – equilibrium fractionation coefficient, $\varepsilon_{eq} = \alpha_{eq} - 1$

ε_{kin} - kinetic fractionation coefficient. $\varepsilon_{kin} = \alpha_{kin} - 1$.

570 It can be shown (Gat, 2001; Horita et al., 2008) that kinetic fractionation coefficient is a linear function of the relative humidity deficit in the ambient atmosphere:

$$\varepsilon_{kin} = n \cdot \varepsilon_{diff} (1 - h_N) \quad (5)$$

575 where n stands for numerical factor, called turbulence parameter, varying in the range from zero to one, h_N signify relative humidity normalized to the temperature of the evaporating water body, whereas ε_{diff} is the kinetic fractionation coefficient associated with diffusion of water isotopologues in air.

580 The value of n is controlled mainly by wind conditions prevailing over the evaporating surface. It quantifies apparent reduction of the diffusive fractionation coefficient ε_{diff} due to impact of turbulent transport. The value of $n = 0.5$, was adopted in the calculations, following the results of laboratory experiments with evaporation of water drops in humid atmosphere reported by Steward (1975). The value of F parameter for each analyzed event was assessed based on the same publication (Stewart, 1975) (Fig. 4) assuming drop radius equal 1 mm. Travel time of raindrops drops from the cloud base to the surface was derived from the position of LCL level and the terminal velocity of drops, both reported for the analyzed events in Table 1. It was further assumed in the calculations that the difference between drop temperature and ambient air temperature is small, thus allowing to use ambient humidity instead to normalized humidity. Although this assumption may result in an over-estimation of the impact of partial evaporation of raindrops on their isotope characteristics, we think that the effect will be
585 small hue to high ambient relative humidities (>90%) used in the calculations.

590 The results of the calculations outlined above are summarized in Table 2. It is clear that for atmospheric conditions prevailing during rainy period, represented by 2020/02/10 night-time convective event, the degree of partial evaporation of raindrops below the cloud base is negligible (reduction of the mean d -excess value in the order of 0.1%). This stems mainly from the low elevation of the mean cloud level above the local ground and the resulting short travel time of raindrops to the surface, as well as very high relative humidity of ambient atmosphere below the cloud base. In contrast, the calculations preformed for the 24/02/2021 day-time event indicate that, for the situations with relatively high elevation of the cloud base level and low ambient relative humidity of the atmosphere beneath this level, the impact of partial evaporation of raindrops on their isotope characteristics can be substantial.

4 Concluding remarks

595 This~~This~~ The results of this work provides a new perspective on~~provide deeper insights into the mechanisms controlling~~ the isotopic variability of convective rainfall in the inland~~high of Brazil~~ tropics.~~We combined high of Brazil.~~ High-frequency sampling of rainfall, covering a 1.5-year period (September 2019 – February 2021), was combined~~with~~ extensive monitoring of meteorological parameters inof~~of~~ the local atmosphere, satellite imagery and HYSPLIT backward trajectory modelling of moist air masses bringing rainfall- the Rio Claro site, a continental, tropical location in the south-eastern Brazil. In total, 90 samples representing
600 eight convective events covering three seasons (summer, autumn and spring) have been collected and analyzed.

Formatado: Fonte: Não Negrito

605 On the monthly time scale, the Rio Claro site reveals typical variability observed in other tropical sites, with high amount of rainfall during the rainy period, strongly depleted in heavy isotopes, and high δ values during the dry period. ~~High-frequency, intra-event sampling implemented in this work revealed an unexpected characteristic of the sampled convective rainfall fractions. A distinct diurnal variability was discovered, with large differences in the δ values and the d excess parameter between the daytime and night time rainfall fractions. A conceptual model, based on local high-frequency meteorological observations, satellite imagery and HYSPLIT modelling was proposed to explain the observed diurnal variations of the isotopic composition of the collected rainfall fractions. We suggest that the observed diurnal variability is largely caused by local effects, i.e. the differences in the convective clouds structure, rain-producing systems during daytime and night time causing large changes in the isotope signatures of daytime rainfall due to partial evaporation of raindrops below the cloud-base level and apparent absence of those effects for night time rainfall fractions.~~ The high-frequency isotope and meteorological data gathered in this study allowed to address the reasons of this strong seasonal variability of isotope characteristics of convective rainfall in some detail. The isotope characteristics of the analysed events representing the rainy period, combined with dedicated Hysplit modelling of moist air masses associated with those events, suggest that overwhelming majority rainfall falling in south-eastern Brazil during austral summer is generated by moist air masses originating in the equatorial Atlantic Ocean. They pass the entire Amazon basin from east to west, interacting on the way with the rainforest through intense moisture recycling. Deflected by the Andes, they continue to the southeastern Brazil where they lose their high moisture load. It is hard to overestimate the importance of this regional atmospheric moisture transport scheme for the southeastern Brazil in the context of ongoing deforestation of the Amazon rainforest and progressing climate change. Possible weakening of the extent of moisture recycling over the Amazon rainforest may result in substantial reduction of precipitation amount in southeastern Brazil, with grave consequences for the Brazilian economy.

615 ~~Day-night differences and diurnal cycle in water isotopic composition of convective systems presented here offers an interesting new perspective for the ongoing discussion of the ‘amount effect’ in tropical areas.~~

625 ~~Peculiar isotope characteristics of the autumn and spring rainfall events analysed in this study, combined with dedicated Hysplit modelling of backward trajectories of moist air masses, strongly suggest that rainfall associated with the dry period in the region, largely originates from moisture of continental origin. This moisture flux is generated in evapotranspiration processes returning water stored in the soil column and in the surface water bodies predominantly during the rainy period. It should be emphasized that isotope characteristics of dry season rainfall provided a decisive argument in this respect.~~

630 ~~Finally, thanks to high-resolution isotope and meteorological data generated in this study, the impact of purely local processes, such as below-cloud partial evaporation of raindrops on the isotopic composition of convective rainfall could be assessed. This semi-quantitative assessment confirmed that under specific conditions (high cloud base position in the local atmosphere, moderate or low relative humidity of ambient relative humidity of the atmosphere beneath this level), the impact of partial evaporation of raindrops on their isotope characteristics can be substantial.~~

Although high-frequency rainfall sampling is logistically difficult, we encourage future studies of this type in different geographical regions across the tropics, to ~~search for diurnal variations in~~ better understand the factors controlling the isotopic

635 composition of convective rainfall during rainy period. Such studies should be accompanied by extensive monitoring of local
640 meteorological parameters and modelling of regional transport of moisture to the rainfall collection site.

Financial support

This work was funded by grants the São Paulo Research Foundation (FAPESP) under Processes 2018/06666-4, 2019/03467-
640 3 and 2021/10538-4, and by the International Atomic Energy Agency Grant CRP-F31006.

Acknowledgment

FAPESP support for the scholarship provided under the Process 2019/03467-3 and 2021/10538-4 is acknowledged. Durán-
Quesada acknowledges time for analysis and writing provided within UCR C1038 project.

645 References

Adler, R. F. and Fenn, D. D.: Thunderstorm Vertical Velocities Estimated from Satellite Data, *American*, 36, 1747–1754, [https://doi.org/10.1175/1520-0469\(1979\)036,1747: TVVEFS.2.0.CO;2](https://doi.org/10.1175/1520-0469(1979)036<1747:TVVEFS.2.0.CO;2), 1979.

Adler, R. F. and Mack, R. A.: Thunderstorm Cloud Top Dynamics as Inferred from Satellite Observations and a Cloud Top
Parcel Model, *American Meteorological Society*, 43, 1945–1960, [https://doi.org/10.1175/1520-
650 0469\(1986\)043,1945:TCTDAI.2.0.CO;2](https://doi.org/10.1175/1520-0469(1986)043,1945:TCTDAI.2.0.CO;2), 1986.

Aemisegger, F., Spiegel, J. K., Pfahl, S., Sodemann, H., Eugster, W., and Wernli, H.: Isotope meteorology of cold front
passages: A case study combining observations and modeling, *Geophysical Research Letters*, 42, 5652–5660,
<https://doi.org/10.1002/2015GL063988>, 2015a, 2015.

~~Aemisegger, F., Spiegel, J. K., Pfahl, S., Sodemann, H., Eugster, W., and Wernli, H.: Isotope meteorology of cold front
655 passages: A case study combining observations and modeling, *Geophysical Research Letters*, 42, 5652–5660,
<https://doi.org/10.1002/2015GL063988>, 2015b.~~

Aggarwal, P. K., Romatschke, U., Araguas-Araguas, L., Belachew, D., Longstaffe, F. J., Berg, P., Schumacher, C., and Funk,
A.: Proportions of convective and stratiform precipitation revealed in water isotope ratios, *Nature Geoscience*, 9, 624–629,
<https://doi.org/10.1038/ngeo2739>, 2016.

660 [Barras, V. and Simmonds, I.: Observation and modeling of stable water isotopes as diagnostics of rainfall dynamics over
southeastern Australia, *Journal of Geophysical Research Atmospheres*, 114, <https://doi.org/10.1029/2009JD012132>, 2009.](#)

Celle-Jeanton, H., Gonfiantini, R., Travi, Y., and Sol, B.: Oxygen-18 variations of rainwater during precipitation: Application
of the Rayleigh model to selected rainfalls in Southern France, *Journal of Hydrology*, 289, 165–177,
<https://doi.org/10.1016/j.jhydrol.2003.11.017>, 2004.

665 Coplen, T. B., Neiman, P. J., White, A. B., Landwehr, J. M., Ralph, F. M., and Dettinger, M. D.: Extreme changes in stable
hydrogen isotopes and precipitation characteristics in a landfalling Pacific storm, *Geophysical Research Letters*, 35, L21808,

Formatado: Recuo: À esquerda: 0 cm, Primeira linha: 0 cm

Formatado: Recuo: À esquerda: 0 cm, Primeira linha: 0 cm

Formatado: Recuo: À esquerda: 0 cm, Primeira linha: 0 cm

<https://doi.org/10.1029/2008GL035481>, 2008.

[Craig, H. and Gordon, L. I.: Deuterium and oxygen 18 variations in the ocean and the marine atmosphere., edited by: Tongiorgi, E., Stable isotopes in oceanographic and paleotemperatures, Pisa, 9–130 pp., 1965.](#)

670 [Cuntz, M., Ogé, J., Farquhar, G. D., Peylin, P., and Cernusak, L. A.: Modelling advection and diffusion of water isotopologues in leaves, Plant, Cell and Environment, 30, 892–909, <https://doi.org/10.1111/j.1365-3040.2007.01676.x>, 2007.](#)

Dansgaard, W.: Stable isotopes in precipitation, Tellus, 16, 436–468, <https://doi.org/10.3402/tellusa.v16i4.8993>, 1964.

Donat, M. G., Alexander, L. V., Yang, H., Durre, I., Vose, R., Dunn, R. J. H., Willett, K. M., Aguilar, E., Brunet, M., Caesar, J., Hewitson, B., Jack, C., Klein Tank, A. M. G., Kruger, A. C., Marengo, J., Peterson, T. C., Renom, M., Oria Rojas, C.,

675 [Rusticucci, M., Salinger, J., Elrayah, A. S., Sekele, S. S., Srivastava, A. K., Trewin, B., Villarroel, C., Vincent, L. A., Zhai, P., Zhang, X., and Kitching, S.: Updated analyses of temperature and precipitation extreme indices since the beginning of the twentieth century: The HadEX2 dataset, Journal of Geophysical Research Atmospheres, 118, 2098–2118, <https://doi.org/10.1002/jgrd.50150>, 2013.](#)

[Dongmann, G. and Nürnberg, H. W.: On the Enrichment of H2180 in the Leaves of Transpiring Plants, Radiation and Environmental Biophysics, 52, 41–52, 1974.](#)

680 [Endries, J. L., Perry, L. B., Yuter, S. E., Seimon, A., Andrade-Flores, M., Winkelmann, R., Quispe, N., Rado, M., Montoya, N., Velarde, F., and Arias, S.: Radar-observed characteristics of precipitation in the tropical high andes of Southern Peru and Bolivia, Journal of Applied Meteorology and Climatology, 57, 1441–1458, <https://doi.org/10.1175/JAMC-D-17-0248.1>, 2018.](#)

[van der Ent, R. J. and Tuinenburg, O. A.: The residence time of water in the atmosphere revisited, Hydrology and Earth System Sciences, 21, 779–790, <https://doi.org/10.5194/hess-21-779-2017>, 2017.](#)

685 [Flanagan, L. B., Comstock, J. P., and Ehleringer, J. R.: Comparison of modeled and observed environmental influences on the stable oxygen and hydrogen isotope composition of leaf water in Phaseolus vulgaris L. Plant Physiology, 96, 588–596, <https://doi.org/10.1104/pp.96.2.588>, 1991.](#)

[Froehlich, K., Gibson, J. J., and Aggarwal, P.: Deuterium excess in precipitation and its climatological significance, Journal of Geophysical Research-Atmospheres, 1–23, 2002.](#)

690 [Gadgil, S.: The Indian monsoon and its variability, Annual Review of Earth and Planetary Sciences, 31, 429–467, <https://doi.org/10.1146/annurev.earth.31.100901.141251>, 2003.](#)

[García-Santos, S., Sánchez-Murillo, R., Peña-Paz, T., Chirinos-Escobar, M. J., Hernández-Ortiz, J. O., Mejía-Escobar, E. J., and Ortega, L.: Water stable isotopes reveal a complex rainfall to groundwater connectivity in central Honduras, Science of the Total Environment, 844, <https://doi.org/10.1016/j.scitotenv.2022.156941>, 2022.](#)

695 [Garreaud, R. D.: Cold air incursions over subtropical South America: Mean structure and dynamics, Monthly Weather Review, 128, 2544–2559, \[https://doi.org/10.1175/1520-0493\\(2000\\)128<2544:caioss>2.0.co;2\]\(https://doi.org/10.1175/1520-0493\(2000\)128<2544:caioss>2.0.co;2\), 2000.](#)

[Gat, J. R., & Matsui, E.: Atmospheric water balance in the Amazon Basin: An isotopic evapotranspiration model, Journal of Geophysical Research, 96, 13179–13188, <https://doi.org/https://doi.org/10.1029/91JD00054>, 1991.](#)

700 [Gat, J. R.: Environmental isotopes in the hydrological cycle: Principles and applications. Volume II, Atmospheric water,](#)

Formatado: Recuo: À esquerda: 0 cm, Primeira linha: 0 cm

Formatado: Recuo: À esquerda: 0 cm, Primeira linha: 0 cm

Formatado: Recuo: À esquerda: 0 cm, Primeira linha: 0 cm

[Technical documents in hydrology, Paris, 1–113 pp., 2001.](#)

[Gedzelman, S. D. and Lawrence, J. R.: The Isotopic Composition of Precipitation from Two Extratropical Cyclones, *American Meteorological Society*, 118, 495–509, \[https://doi.org/10.1175/1520-0493\\(1990\\)118.0495:TICOPF.2.0.CO;2\]\(https://doi.org/10.1175/1520-0493\(1990\)118.0495:TICOPF.2.0.CO;2\), 1990.](#)

705 Gimeno, L., Drumond, A., Nieto, R., Trigo, R. M., and Stohl, A.: On the origin of continental precipitation, *Geophysical Research Letters*, 37, 1–7, <https://doi.org/10.1029/2010GL043712>, 2010.

[Gimeno, L., Vázquez, M., Eiras-Barca, J., Sorí, R., Stojanovic, M., Algarra, I., Nieto, R., Ramos, A. M., Durán-Quesada, A. M., and Dominguez, F.: Recent progress on the sources of continental precipitation as revealed by moisture transport analysis, *Earth-Science Reviews*, 201, 103070, <https://doi.org/10.1016/j.earscirev.2019.103070>, 2020.](#)

710 [Gonfiantini, R.: Environmental isotopes in lake studies, in: *Handbook of Environmental Isotope Geochemistry Vol. 2 The Terrestrial Environment, vol. 2*, Elsevier, Amsterdam, 113–168, 1986.](#)

Graf, P., Wernli, H., Pfahl, S., and Sodemann, H.: A new interpretative framework for below-cloud effects on stable water isotopes in vapour and rain, *Atmospheric Chemistry and Physics*, 19, 747–765, <https://doi.org/10.5194/acp-19-747-2019>, 2019.

715 Han, X., Lang, Y., Wang, T., Liu, C.-Q., Li, F., Wang, F., Guo, Q., Li, S., Liu, M., Wang, Y., and Xu, A.: Temporal and spatial variations in stable isotopic compositions of precipitation during the typhoon Lekima (2019), China, *Science of The Total Environment*, 762, 143143, <https://doi.org/10.1016/j.scitotenv.2020.143143>, 2021.

[Horita, J. and Wesolowski, D. J.: Horita and Wesolowski 1994, *Geochimica et Cosmochimica Acta*, 58, 1–13, 1994.](#)

[Horita, J., Rozanski, K., and Cohen, S.: Isotope effects in the evaporation of water: a status report of the Craig–Gordon model, *Isotopes in Environmental and Health Studies*, 44, 23–49, <https://doi.org/10.1080/10256010801887174>, 2008.](#)

720 Houze, R.: Stratiform precipitation in regions of convection: A Meteorological Paradox?, *Bulletin of the American Meteorological Society*, 78, 2179–2195, 1997.

Houze, R. A.: *Cloud dynamics*, Academic Press Limited, 573 pp., [https://doi.org/10.1016/0377-0265\(87\)90017-0](https://doi.org/10.1016/0377-0265(87)90017-0), 1993.

Houze, R. A.: *Mesoscale Convective Systems*, in: *International Geophysics*, vol. 104, 237–286, <https://doi.org/10.1016/B978-0-12-374266-7.00009-3>, 2004.

725 [Houze, R. A. J.: Observed structure of mesoscale convective systems and implications for large-scale heating., *Quart. J. Roy. Meteor. Soc.*, 115, 425–461, 1989.](#)

Hu, J., Emile-Geay, J., Nusbaumer, J., and Noone, D.: Impact of Convective Activity on Precipitation $\delta^{18}\text{O}$ in Isotope-Enabled General Circulation Models, *Journal of Geophysical Research: Atmospheres*, 123, 13,595–13,610, <https://doi.org/10.1029/2018JD029187>, 2018.

730 [Hu, J., Bailey, A., Nusbaumer, J., Dec, S., Sasser, C., and Worden, J.: Tracking Shallow Convective Mixing and Its Influence on Low-Level Clouds With Stable Water Isotopes in Vapor, *Journal of Geophysical Research: Atmospheres*, 127, <https://doi.org/10.1029/2021JD035355>, 2022.](#)

[IAEA: IAEA / GNIP precipitation sampling guide V2.02, *Global Network of Isotopes in Precipitation \(GNIP\)*, 20, 2014.](#)

IPCC, W. G. I.-T. P. S. B.: *Regional fact sheet – Central and South America*, Sixth Assessment Report, 1–2 pp., 2021.

Formatado: Recuo: À esquerda: 0 cm, Primeira linha: 0 cm

Formatado: Recuo: À esquerda: 0 cm, Primeira linha: 0 cm

Formatado: Recuo: À esquerda: 0 cm, Primeira linha: 0 cm

Formatado: Recuo: À esquerda: 0 cm, Primeira linha: 0 cm

Formatado: Recuo: À esquerda: 0 cm, Primeira linha: 0 cm

735 Jeelani, G., Deshpande, R. D., Galkowski, M., and Rozanski, K.: Isotopic composition of daily precipitation along the southern foothills of the Himalayas: Impact of marine and continental sources of atmospheric moisture, *Atmospheric Chemistry and Physics*, 18, 8789–8805, <https://doi.org/10.5194/acp-18-8789-2018>, 2018.

Klaassen, W.: Radar Observations and Simulation of the Melting Layer of Precipitation, *Journal of the Atmospheric Sciences*, 45, 3741–3753, 1988.

740 Kodama, Y.: Large-scale common features of subtropical precipitation zones (the Baiu Frontal Zone , the SPCZ , and the SACZ) Part I: Characteristics of subtropical frontal zones, *Journal of the Meteorological Society of Japan*, 70, 813–836, <https://doi.org/10.1248/cpb.37.3229>, 1992.

~~Kruskal, W. H. and Wallis, W. A.: Use of Ranks in One-Criterion Variance Analysis, *Journal of the American Statistical Association*, 47, 583–621, 1952.~~

745 Kurita, N.: Water isotopic variability in response to mesoscale convective system over the tropical ocean, *Journal of Geophysical Research Atmospheres*, 118, ~~10376–10390~~, <https://doi.org/10.1002/jgrd.50754>, ~~2013a~~.

~~Kurita, N.: Water isotopic variability in response to mesoscale convective system over the tropical ocean, *Journal of Geophysical Research Atmospheres*, 118, 10,376-10,390, <https://doi.org/10.1002/jgrd.50754>, 2013b~~

750 Lawrence, J. R., Gedzelman, S. D., Dexheimer, D., Cho, H. K., Carrie, G. D., Gasparini, R., Anderson, C. R., Bowman, K. P., and Biggerstaff, M. I.: Stable isotopic composition of water vapor in the tropics, *Journal of Geophysical Research-Atmospheres*, 109, 16, <https://doi.org/D0611510.1029/2003jd004046>, 2004.

Lee, J. and Fung, I.: “Amount effect” of water isotopes and quantitative analysis of post-condensation processes, *Hydrological Processes*, 22, 1–8, <https://doi.org/10.1002/hyp.6637>, 2008.

755 Lekshmy, P. R., Midhun, M., Ramesh, R., and Jani, R. A.: 18 O depletion in monsoon rain relates to large scale organized convection rather than the amount of rainfall, *Scientific Reports*, 4, 1–5, <https://doi.org/10.1038/srep05661>, 2014.

Luiz Silva, W., Xavier, L. N. R., Maceira, M. E. P., and Rotunno, O. C.: Climatological and hydrological patterns and verified trends in precipitation and streamflow in the basins of Brazilian hydroelectric plants, *Theoretical and Applied Climatology*, 137, 353–371, <https://doi.org/10.1007/s00704-018-2600-8>, 2019.

760 Machado, L. A. T. and Laurent, H.: ~~The convective system area expansion over Amazonia and its relationships with convective system life duration and high-level wind divergence, *Monthly Weather Review*, 132, 714–725, [https://doi.org/10.1175/1520-0493\(2004\)132<0714:TCSAEO>2.0.CO;2](https://doi.org/10.1175/1520-0493(2004)132<0714:TCSAEO>2.0.CO;2), 2004.~~

~~Machado, L. A. T. and Rossow, W. B.: Structural Characteristics and Radiative Properties of Tropical Cloud Clusters, *Monthly Weather Review*, 121, 3234–3260, 1993.~~

765 Machado, L. A. T., Rossow, W. B., Guedes, R. L., and Walker, A. W.: Life cycle variations of mesoscale convective systems over the Americas, *Monthly Weather Review*, 126, 1630–1654, [https://doi.org/10.1175/1520-0493\(1998\)126<1630:LCVOMC>2.0.CO;2](https://doi.org/10.1175/1520-0493(1998)126<1630:LCVOMC>2.0.CO;2), 1998.

~~Managave, S. R., Jani, R. A., Narayana Rao, T., Sunilkumar, K., Satheshkumar, S., and Ramesh, R.: Intra-event isotope and raindrop size data of tropical rain reveal effects concealed by event-averaged data, *Climate Dynamics*, 47, 981–987,~~

Formatado: Recuo: À esquerda: 0 cm, Primeira linha: 0 cm

Formatado: Recuo: À esquerda: 0 cm, Primeira linha: 0 cm

<https://doi.org/10.1007/s00382-015-2884-7>, 2016.

770 Marengo, J. A., Soares, W. R., Saulo, C., and Nicolini, M.: Climatology of the low-level jet east of the Andes as derived from
the NCEP-NCAR reanalyses: Characteristics and temporal variability, *Journal of Climate*, 17, 2261–2280,
[https://doi.org/10.1175/1520-0442\(2004\)017<2261:COTLJE>2.0.CO;2](https://doi.org/10.1175/1520-0442(2004)017<2261:COTLJE>2.0.CO;2), 2004.

Marengo, J. A., Ambrizzi, T., Alves, L. M., Barreto, N. J. C., Simões Reboita, M., and Ramos, A. M.: Changing Trends in
Rainfall Extremes in the Metropolitan Area of São Paulo: Causes and Impacts, *Frontiers in Climate*, 2, 1–13,
775 <https://doi.org/10.3389/fclim.2020.00003>, 2020.

Mehta, S., Mehta, S. K., Singh, S., Mitra, A., Ghosh, S. K., and Raha, S.: Characteristics of the Z–R Relationships Observed
Using Micro Rain Radar (MRR-2) over Darjeeling (27.05° N, 88.26° E): A Complex Terrain Region in the Eastern Himalayas,
Pure and Applied Geophysics, 177, 4521–4534, <https://doi.org/10.1007/s00024-020-02472-6>, 2020.

Moerman, J. W., Cobb, K. M., Adkins, J. F., Sodemann, H., Clark, B., and Tuen, A. A.: Diurnal to interannual rainfall $\delta^{18}O$
780 variations in northern Borneo driven by regional hydrology, *Earth and Planetary Science Letters*, 369–370, 108–119,
<https://doi.org/10.1016/j.epsl.2013.03.014>, 2013.

Muller, C. L., Baker, A., Fairchild, I. J., Kidd, C., and Boomer, I.: Intra-Event Trends in Stable Isotopes: Exploring Midlatitude
Precipitation Using a Vertically Pointing Micro Rain Radar, *Journal of Hydrometeorology*, 16, 194–213,
<https://doi.org/10.1175/JHM-D-14-0038.1>, 2015.

785 Munksgaard, N. C., Zwart, C., Haig, J., Cernusak, L. A., and Bird, M. I.: Coupled rainfall and water vapour stable isotope time
series reveal tropical atmospheric processes on multiple timescales, *Hydrological Processes*, 34, 111–124,
<https://doi.org/10.1002/hyp.13576>, 2020.

~~Nicolini, M., Saulo, A. C., Torres, J. C., and Salio, P.: Enhanced Precipitation Over Southeastern South America Related To
Strong Low Level Jet Events During Austral Warm Season, *Meteorologica*, 27, 59–69, 2002.~~

790 ~~R-Core Team: A language and environment for statistical computing. R Foundation for Statistical Computing, Vienna, Austria.
<https://www.R-project.org/>, 2022.~~

Rao, N. T., Kirankumar, N. V. P., Radhakrishna, B., and Rao, N. D.: Classification of tropical precipitating systems using
wind profiler spectral moments. Part I: Algorithm description and validation, *Journal of Atmospheric and Oceanic Technology*,
25, 884–897, <https://doi.org/10.1175/2007JTECHA1031.1>, 2008.

795 Ribeiro, B. Z., Machado, L. A. T., Biscaro, T. S., Freitas, E. D., Mozer, K. W., and Goodman, S. J.: An evaluation of the
GOES-16 rapid scan for nowcasting in southeastern Brazil: Analysis of a severe hailstorm case, *Weather and Forecasting*, 34,
1829–1848, <https://doi.org/10.1175/WAF-D-19-0070.1>, 2019.

Risi, C., Bony, S., Vimeux, F., ~~Deseroix, L., Ibrahim, B., Lebreton, E., Mamadou, I, Chongd, M., and Sultan, B.: What controls
the Deseroix, L.: Evolution of the stable water isotopic composition of the African monsoon precipitation? Insights from
800 event-based precipitation collected during rain sampled along Sahelian squall lines, *Quarterly Journal of the 2006 AMMA field
campaign, — Geophysical Research Letters, — 35, — 1–6* Royal Meteorological Society, 136, 227–242,
<https://doi.org/10.1029/2008GL035920>, 2008/1002/qj.485, 2010.~~

Formatado: Recuo: À esquerda: 0 cm, Primeira linha: 0 cm

Formatado: Recuo: À esquerda: 0 cm, Primeira linha: 0 cm

~~Risi, C., Galewsky, J., Reverdin, G., and Briant, F.: Controls on the water vapor isotopic composition near the surface of tropical oceans and role of boundary layer mixing processes, 20, 1–37, 2019.~~

805 Roberts, R. D. and Rutledge, S.: Nowcasting storm initiation and growth using GOES-8 and WSR-88D data, Weather and Forecasting, 18, 562–584, [https://doi.org/10.1175/1520-0434\(2003\)018<0562:NSIAGU>2.0.CO;2](https://doi.org/10.1175/1520-0434(2003)018<0562:NSIAGU>2.0.CO;2), 2003.

Romatschke, U. and Houze, R. A.: Extreme summer convection in South America, Journal of Climate, 23, 3761–3791, <https://doi.org/10.1175/2010JCLI3465.1>, 2010.

810 Romatschke, U. and Houze, R. A.: Characteristics of precipitating convective systems accounting for the summer rainfall of tropical and subtropical South America, Journal of Hydrometeorology, 14, 25–46, <https://doi.org/10.1175/JHM-D-12-060.1>, 2013.

Rozanski, K., Sonntag, C., and Munnich, K. O.: Factors controlling stable isotope composition of European precipitation., Tellus, 34, 142–150, <https://doi.org/10.3402/tellusa.v34i2.10796>, 1982.

815 Rozanski, K., Araguás-Araguás, L., and Gonfiantini, R.: Isotopic Patterns in Modern Global Precipitation, 1–36, <https://doi.org/10.1029/GM078p0001>, 1993.

~~Rozanski, K., Mook, W. G., and Froehlich, K.: Environmental Isotopes in the Hydrological Cycle: Principles and Applications., Technical documents in hydrology, Paris, 1–117 pp., 2001.~~

~~Salati, E., Dall'Olio, A., Matsui, E., and Gat, J. R.: Recycling of water in the Amazon Basin: An isotopic study, Water Resources Research, 15, 1250–1258, <https://doi.org/10.1029/WR015i005p01250>, 1979.~~

820 Sánchez-Murillo, R., Durán-Quesada, A. M., Birkel, C., Esquivel-Hernández, G., and Boll, J.: Tropical precipitation anomalies and d-excess evolution during El Niño 2014–16, Hydrological Processes, 31, 956–967, <https://doi.org/10.1002/hyp.11088>, 2017.

825 Sánchez-Murillo, R., Durán-Quesada, A. M., Esquivel-Hernández, G., Rojas-Cantillano, D., Birkel, C., Welsh, K., Sánchez-Llull, M., Alonso-Hernández, C. M., Tetzlaff, D., Soulsby, C., Boll, J., Kurita, N., and Cobb, K. M.: Deciphering key processes controlling rainfall isotopic variability during extreme tropical cyclones, Nature Communications, 10, 1–10, <https://doi.org/10.1038/s41467-019-12062-3>, 2019.

~~Dos Santos, V., Gastmans, D., Sánchez-Murillo, R., Gozzo, L. F., Batista, L. V., Manzione, R. L., and Martinez, J.: Regional atmospheric dynamics govern interannual and seasonal stable isotope composition in southeastern Brazil, Journal of Hydrology, 579, 124136, <https://doi.org/10.1016/j.jhydrol.2019.124136>, 2019.~~

830 dos Santos, V., Marshall Fleming, P., Henrique Mancini, L., Dalva Santos Cota, S., de Lima, G. B., Rodrigues Gomes, R., Kirchheim, R. E., Sánchez-Murillo, R., and Gastmans, D.: Distinguishing the Regional Atmospheric Controls on Precipitation Isotopic Variability in the Central-Southeast Portion of Brazil, Advances in Atmospheric Sciences, 39, 1693–1708, <https://doi.org/10.1007/s00376-022-1367-0>, 2022.

835 ~~Saulo, a. C., Nicolini, M., and Chou, S. C.: Model characterization of the South American low level flow during the 1997–1998 spring-summer season, Climate Dynamics, 16, 867–881, <https://doi.org/10.1007/s003820000085>, 2000.~~

~~dos Santos, V., Gastmans, D., and Sánchez-Murillo, R.: Isotope and meteorologic database of high-frequency sampling of~~

Formatado: Recuo: À esquerda: 0 cm, Primeira linha: 0 cm

Formatado: Recuo: À esquerda: 0 cm, Primeira linha: 0 cm

Formatado: Recuo: À esquerda: 0 cm, Primeira linha: 0 cm

[convective rainfall events in Rio Claro, Brazil, https://doi.org/10.17632/kk3gs8zn4s.1, 2023.](https://doi.org/10.17632/kk3gs8zn4s.1)

Schmit, T. J., Griffith, P., Gunshor, M. M., Daniels, J. M., Goodman, S. J., and Lehair, W. J.: A closer look at the ABI on the goes-r series, *Bulletin of the American Meteorological Society*, 98, 681–698, <https://doi.org/10.1175/BAMS-D-15-00230.1>, 2017.

Schumacher, C. and Houze, R. A.: Stratiform rain in the tropics as seen by the TRMM precipitation radar, *Journal of Climate*, 16, 1739–1756, [https://doi.org/10.1175/1520-0442\(2003\)016<1739:SRITTA>2.0.CO;2](https://doi.org/10.1175/1520-0442(2003)016<1739:SRITTA>2.0.CO;2), 2003.

[Shapiro, S. S.; Wilk, M. B.: An analysis of variance test for normality \(complete samples\), *Biometrika*, 53, 591–611, 1965.](#)

Siqueira, J. R., Rossow, W. B., Machado, L. A. T., and Pearl, C.: Structural characteristics of convective systems over South America related to cold-frontal incursions, *Monthly Weather Review*, 133, 1045–1064, <https://doi.org/10.1175/MWR2888.1>, 2005.

[Sodemann, H.: Tropospheric transport of water vapour: Lagrangian and Eulerian perspectives, *Swiss Federal Institute of Technology Zurich*, 230 pp., 2006.](#)

Soderberg, K., Good, S. P., O’connor, M., Wang, L., Ryan, K., and Caylor, K. K.: Using atmospheric trajectories to model the isotopic composition of rainfall in central Kenya, *Ecosphere*, 4, 1–18, <https://doi.org/10.1890/ES12-00160.1>, 2013.

Stein, A. F., Draxler, R. R., Rolph, G. D., Stunder, B. J. B., Cohen, M. D., and Ngan, F.: NOAA’s hysplit atmospheric transport and dispersion modeling system, *Bulletin of the American Meteorological Society*, 96, 2059–2077, <https://doi.org/10.1175/BAMS-D-14-00110.1>, 2015.

Steiner, M. and Smith, J. A.: Convective versus stratiform rainfall: An ice-microphysical and kinematic conceptual model, *Atmospheric Research*, 47–48, 317–326, [https://doi.org/10.1016/S0169-8095\(97\)00086-0](https://doi.org/10.1016/S0169-8095(97)00086-0), 1998.

[Stewart, M. K.: Stable isotope fractionation due to evaporation and isotopic exchange of falling waterdrops: Applications to atmospheric processes and evaporation of lakes, *Journal of Geophysical Research*, 80, 1133–1146, https://doi.org/10.1029/JC080i009p01133, 1975.](#)

Sun, C., Shanahan, T. M., and Partin, J.: Controls on the Isotopic Composition of Precipitation in the South-Central United States, *Journal of Geophysical Research: Atmospheres*, 124, 8320–8335, <https://doi.org/10.1029/2018JD029306>, 2019.

Sun, C., Tian, L., Shanahan, T. M., Partin, J. W., Gao, Y., Piatrunia, N., and Banner, J.: Isotopic variability in tropical cyclone precipitation is controlled by Rayleigh distillation and cloud microphysics, *Communications Earth & Environment*, 3, <https://doi.org/10.1038/s43247-022-00381-1>, 2022.

[Taupin, J.-D., Gallaire, R., and Arnaud, Y.: Analyses isotopiques et chimiques des précipitations sahélienne de la région de Niamey au Niger: implications climatologiques, *Hydrochemistry*, 151–162, 1997.](#)

Tharammal, T., G. Bala, and D. N.: Impact of deep convection on the isotopic amount effect in tropical precipitation, *Journal of Geophysical Research Atmospheres*, 122, 1505–1523, <https://doi.org/10.1002/2016JD025555>, 2017.

[Vera, C., Baez, J., Douglas, M., Emmanuel, C. B., Marengo, J., Meitin, J., Nicolini, M., Noguez Paegle, J., Paegle, J., Penalba, O., Salio, P., Saulo, C., Silva Dias, M. A., Silva Dias, P., and Zipser, E.: The South American low-level jet experiment, *Bulletin of the American Meteorological Society*, 87, 63–77, https://doi.org/10.1175/BAMS-87-1-63, 2006.](#)

Formatado: Recuo: À esquerda: 0 cm, Primeira linha: 0 cm

Formatado: Recuo: À esquerda: 0 cm, Primeira linha: 0 cm

Formatado: Recuo: À esquerda: 0 cm, Primeira linha: 0 cm

Formatado: Recuo: À esquerda: 0 cm, Primeira linha: 0 cm

Formatado: Recuo: À esquerda: 0 cm, Primeira linha: 0 cm

Tremoy, G., Vimeux, F., Soumana, S., Souley, I., Risi, C., Favreau, G., and Oï, M.: Clustering mesoscale convective systems with laser-based water vapor $\delta^{18}\text{O}$ monitoring in Niamey (Niger), *Journal of Geophysical Research: Atmospheres*, 119, 5079–5103, <https://doi.org/10.1002/2013JD020968>, 2014.

875 Vila, D. A., Machado, L. A. T., Laurent, H., and Velasco, I.: Forecast and tracking the evolution of cloud clusters (ForTraCC) using satellite infrared imagery: Methodology and validation, *Weather and Forecasting*, 23, 233–245, <https://doi.org/10.1175/2007WAF2006121.1>, 2008.

Vimeux, F., Tremoy, G., Risi, C., and Gallaire, R.: A strong control of the South American SeeSaw on the intra-seasonal variability of the isotopic composition of precipitation in the Bolivian Andes, *Earth and Planetary Science Letters*, 307, 47–58, <https://doi.org/10.1016/j.epsl.2011.04.031>, 2011.

880 Vuille, M., Bradley, R. S., Werner, M., Healy, R., and Keimig, F.: Modeling $\delta^{18}\text{O}$ in precipitation over the tropical Americas: 1. Interannual variability and climatic controls, *Journal of Geophysical Research: Atmospheres*, 108, 1–24, <https://doi.org/10.1029/2001JD002038>, 2003.

885 Wang, S., Zhang, M., Che, Y., Zhu, X., and Liu, X.: Influence of below-cloud evaporation on deuterium excess in precipitation of arid Central Asia and its meteorological controls, *Journal of Hydrometeorology*, 17, 1973–1984, <https://doi.org/10.1175/JHM-D-15-0203.1>, 2016.

Wang, T. and Tang, G.: Spatial Variability and Linkage Between Extreme Convections and Extreme Precipitation Revealed by 22-Year Space-Borne Precipitation Radar Data, *Geophysical Research Letters*, 47, 1–10, <https://doi.org/10.1029/2020GL088437>, 2020.

890 Warner, T. T., Mapes, B. E., and Xu, M.: Diurnal patterns of rainfall in northwestern South America. Part II: Model simulations, *Monthly Weather Review*, 131, 813–829, [https://doi.org/10.1175/1520-0493\(2003\)131<0813:DPORIN>2.0.CO;2](https://doi.org/10.1175/1520-0493(2003)131<0813:DPORIN>2.0.CO;2), 2003.

Winnick, M. J., Chamberlain, C. P., Caves, J. K., and Welker, J. M.: Quantifying the isotopic “continental effect,” *Earth and Planetary Science Letters*, 406, 123–133, <https://doi.org/10.1016/j.epsl.2014.09.005>, 2014.

895 Worden, J., Noone, D., Bowman, K., Beer, R., Eldering, A., Fisher, B., Gunson, M., Goldman, A., Herman, R., Kulawik, S. S., Lampel, M., Osterman, G., Rinsland, C., Rodgers, C., Sander, S., Shephard, M., Webster, C. R., and Worden, H.: Importance of rain evaporation and continental convection in the tropical water cycle, *Nature*, 445, 528–532, <https://doi.org/10.1038/nature05508>, 2007.

World Meteorological Organization: WMO Atlas of Mortality and Economic Losses From Weather, Climate and Water Extremes, 2019 (1970–2019), Geneva 2, Switzerland, 90 pp., 2021.

900 Zilli, M. T., Carvalho, L. M. V., Liebmann, B., and Silva Dias, M. A.: A comprehensive analysis of trends in extreme precipitation over southeastern coast of Brazil, *International Journal of Climatology*, 37, 2269–2279, <https://doi.org/10.1002/joc.4840>, 2017.

Zwart, C., Munksgaard, N. C., Lambrinidis, D., Bird, M. I., Protat, A., and Kurita, N.: The isotopic signature of monsoon conditions, cloud modes, and rainfall type, *Hydrological Processes*, 2296–2303, <https://doi.org/10.1002/hyp.13140>, 2018.

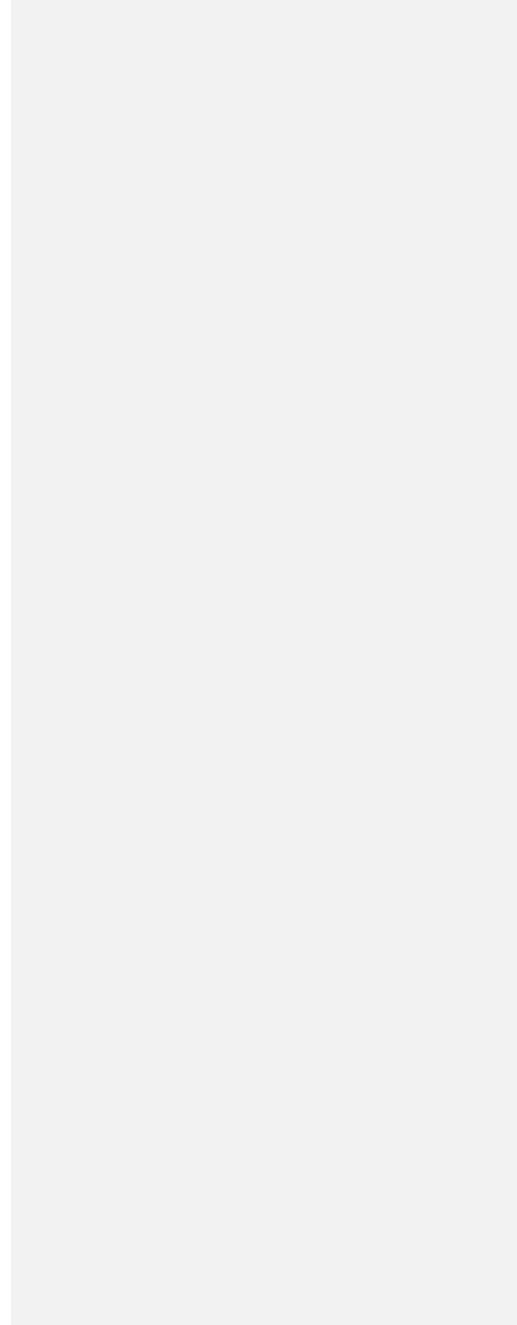
Formatado: Recuo: À esquerda: 0 cm, Primeira linha: 0 cm

Formatado: Recuo: À esquerda: 0 cm, Primeira linha: 0 cm

Formatado: Recuo: À esquerda: 0 cm, Primeira linha: 0 cm

Formatado: Recuo: À esquerda: 0 cm, Primeira linha: 0 cm

905



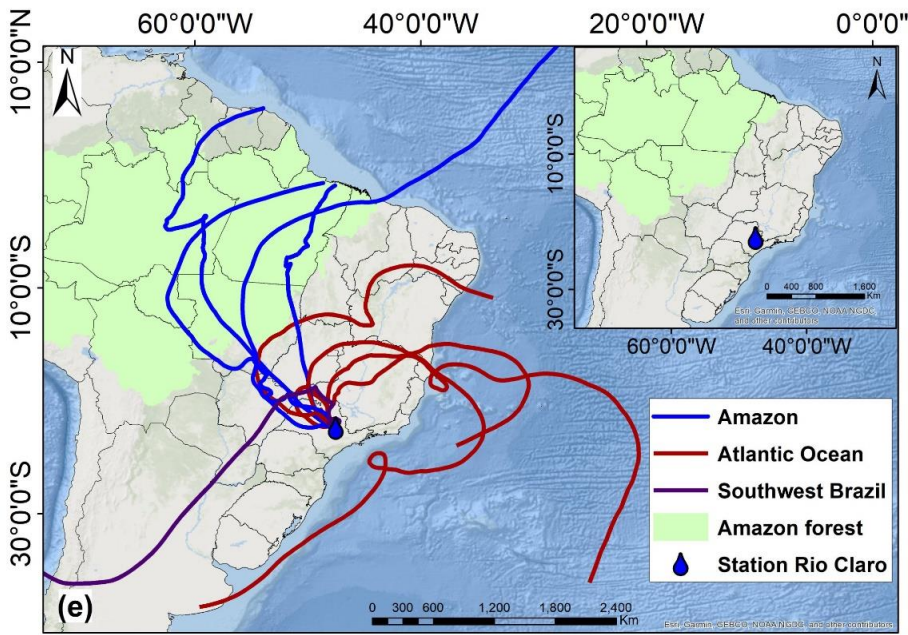
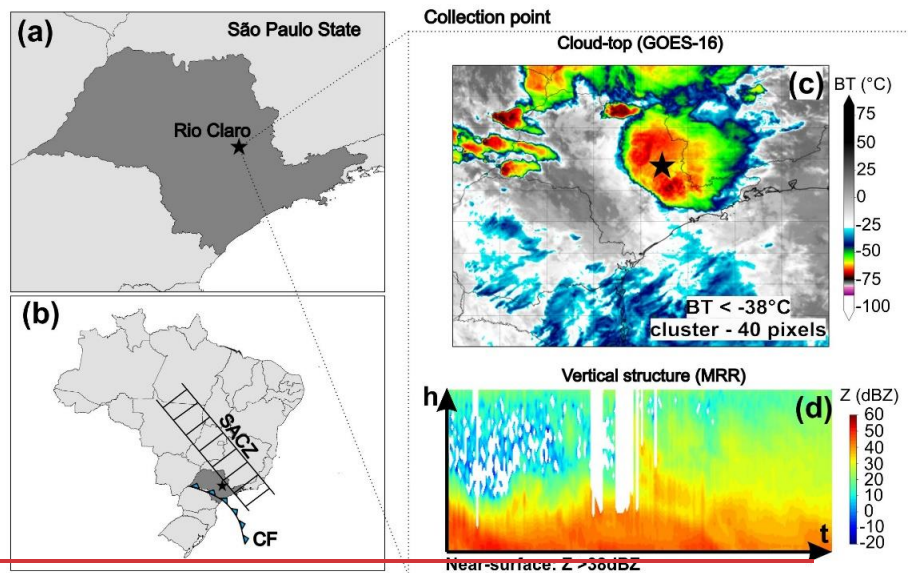


Table 1

Formatado: In
Formatado: F
Formatado: In

Summarizing overall convective rainfall events and median values of isotope and meteorological parameters.

<u>Season</u>	<u>Daytime</u>	<u>Data</u>	<u>Number of samples</u>	<u>Duration</u>	<u>Isotopes</u>			<u>Automatic Weather Station</u>					<u>Micro Rain Radar</u>		<u>GOES- 16</u>
					<u>$\delta^{18}\text{O}$</u>	<u>$\delta^2\text{H}$</u>	<u><i>d</i>-excess</u>	<u>Rain rate</u>	<u>RH</u>	<u>T</u>	<u>Tdw</u>	<u>LCL</u>	<u>Z</u>	<u>w</u>	<u>BT</u>
-	-	-	<u>n</u>	<u>minutes</u>	<u>‰</u>			<u>mm.min⁻¹</u>	<u>%</u>	<u>°C</u>		<u>meters</u>	<u>dBZ</u>	<u>m.s⁻¹</u>	<u>°C</u>
<u>Spring</u>	<u>Day</u>	<u>05/11/2019</u>	<u>21</u>	<u>82</u>	<u>-3.1</u>	<u>0.8</u>	<u>22.9</u>	<u>0.4</u>	<u>96</u>	<u>21</u>	<u>20</u>	<u>146</u>	<u>46</u>	<u>8.0</u>	<u>-63</u>
<u>Spring</u>	<u>Day</u>	<u>18/11/2020</u>	<u>8</u>	<u>141</u>	<u>-4.2</u>	<u>-13.7</u>	<u>19.7</u>	<u>0.2</u>	<u>86</u>	<u>20</u>	<u>17</u>	<u>489</u>	<u>38</u>	<u>7.1</u>	<u>-63</u>
<u>Autumn</u>	<u>Day</u>	<u>09/06/2020</u>	<u>12</u>	<u>96</u>	<u>-3.4</u>	<u>-5.6</u>	<u>17.3</u>	<u>0.3</u>	<u>95</u>	<u>19</u>	<u>18</u>	<u>168</u>	<u>42</u>	<u>7.7</u>	<u>-50</u>
<u>Autumn</u>	<u>Night</u>	<u>23/05/2020</u>	<u>4</u>	<u>131</u>	<u>-2.9</u>	<u>-6.9</u>	<u>16.3</u>	<u>0.0</u>	<u>87</u>	<u>19</u>	<u>17</u>	<u>449</u>	<u>33</u>	<u>6.6</u>	<u>-56</u>
<u>Summer</u>	<u>Night</u>	<u>30/01/2020</u>	<u>6</u>	<u>23</u>	<u>-10.0</u>	<u>-64.4</u>	<u>15.7</u>	<u>0.4</u>	<u>93</u>	<u>23</u>	<u>21</u>	<u>247</u>	<u>38</u>	<u>6.6</u>	<u>-53</u>
<u>Summer</u>	<u>Night</u>	<u>10/02/2020</u>	<u>18</u>	<u>86</u>	<u>-13.9</u>	<u>-92.0</u>	<u>17.5</u>	<u>0.5</u>	<u>97</u>	<u>22</u>	<u>21</u>	<u>93</u>	<u>41</u>	<u>6.7</u>	<u>-39</u>
<u>Summer</u>	<u>Day</u>	<u>01/02/2020</u>	<u>5</u>	<u>18</u>	<u>-10.4</u>	<u>-73.5</u>	<u>13.4</u>	<u>0.6</u>	<u>93</u>	<u>23</u>	<u>21</u>	<u>253</u>	<u>39</u>	<u>7.1</u>	<u>-60</u>
<u>Summer</u>	<u>Day</u>	<u>24/02/2021</u>	<u>16</u>	<u>55</u>	<u>-6.8</u>	<u>-44.8</u>	<u>7.2</u>	<u>0.5</u>	<u>86</u>	<u>21</u>	<u>18</u>	<u>468</u>	<u>35</u>	<u>7.1</u>	<u>-51</u>

RH = Relative Humidity, T = Temperature, Tdw = Dew point temperature, LCL = Lifting condensation level, Z = Reflectivity, w = fall velocity and Brightness temperature.

915 **Table 2.** The results of semi-quantitative assessment of the impact of below-cloud processes on the isotope characteristics of convective precipitation

<u>Rainfall event</u>	<u>T_{INT}^{al}</u> <u>(°C)</u>	<u>RH_{INT}^{bl}</u> <u>(%)</u>	<u>F^c</u> <u>(-)</u>	<u>Δd-excess^d</u> <u>(‰)</u>
The 10/02/2020 event <u>δ_o</u> - isotopic composition of rainfall (‰): <u>δ²H = -91.97, δ¹⁸O = -13.85, d-excess = 18.8</u> <u>δ_A</u> – isotopic composition of equilibrium vapour (‰) ^e : <u>δ²H = -161.6 δ¹⁸O = -23.28, d-excess = 24.6</u>	<u>21.7</u>	<u>98.6</u>	<u>0.9994</u>	<u>0.1</u>
The 24/02/2021 day-time event <u>δ_o</u> - isotopic composition of rainfall (‰): <u>δ²H = -44.8, δ¹⁸O = -6.79, d-excess = 9.5</u> <u>δ_A</u> – isotopic composition of equilibrium vapour (‰): <u>δ²H = -120.3 δ¹⁸O = -16.48, d-excess = 11.5</u>	<u>19.3</u>	<u>93.2</u>	<u>0.9800</u>	<u>3.0</u>

a) mean temperature of below cloud ambient atmosphere (linear interpolation between cloud base and ground level values)

b) mean relative humidity of below cloud ambient atmosphere (linear interpolation between cloud base and ground level values)

920 c) remaining mass fraction of raindrops after their travel from the cloud base to the surface (see text)

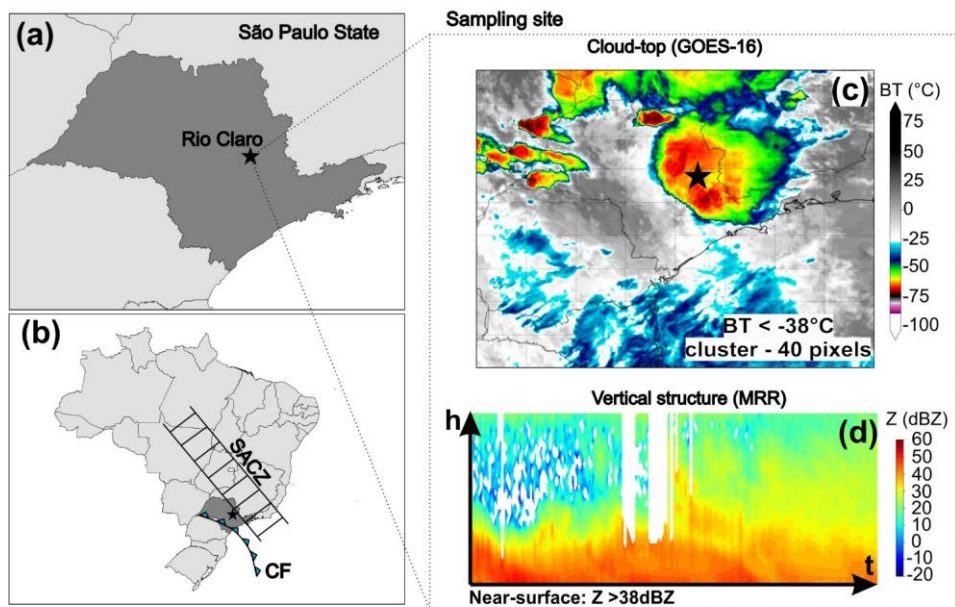
d) reduction of the d-excess of raindrops as a result of their travel from the cloud base to the surface (see text)

e) assumed isotopic composition of ambient humid atmosphere below the cloud base derived from the measured isotopic composition of rainfall and ground-level temperature.

925

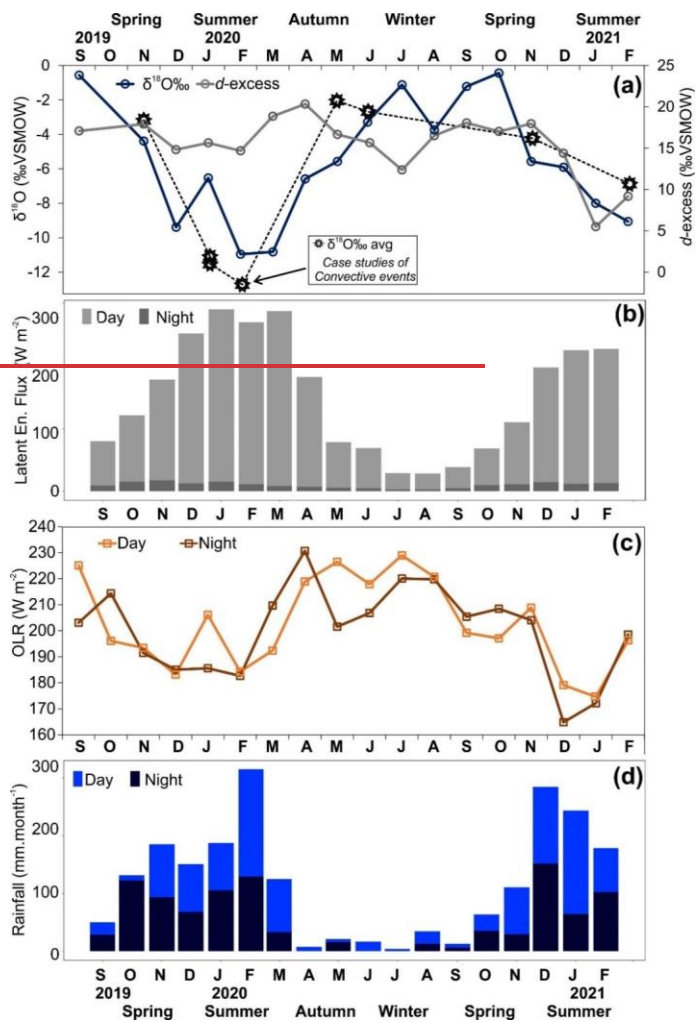
930

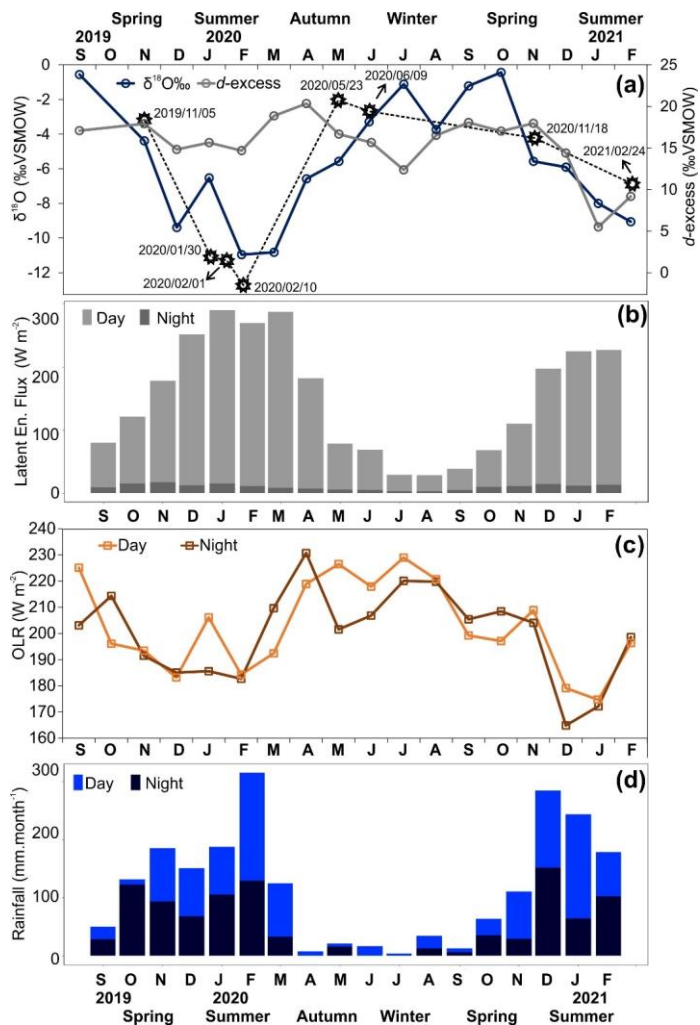
935



940 **Figure 1.** (a) Localization of sampling site in Rio Claro (black star) (b) in regional synoptic context across Brazil and main atmospheric weather systems (CF – cold front and SACZ – Southern Atlantic Convergence Zone). Over collection point (c) GOES-16 satellite imagery showed convective system with lower brightness temperature (BT, cloud-top) and (d) Micro Rain Radar (MRR) illustrates the vertical structure of convective rainfall, height (h) and time (t), characterized by radar reflectivity (Z) with strong values near-surface. (e) transport of atmospheric moisture to the site visualized by air mass back trajectories derived from HYSPLIT modelling. In Figure 1e, the authors used trivial information, the borders of the countries and the ocean provided by the ESRI base map.

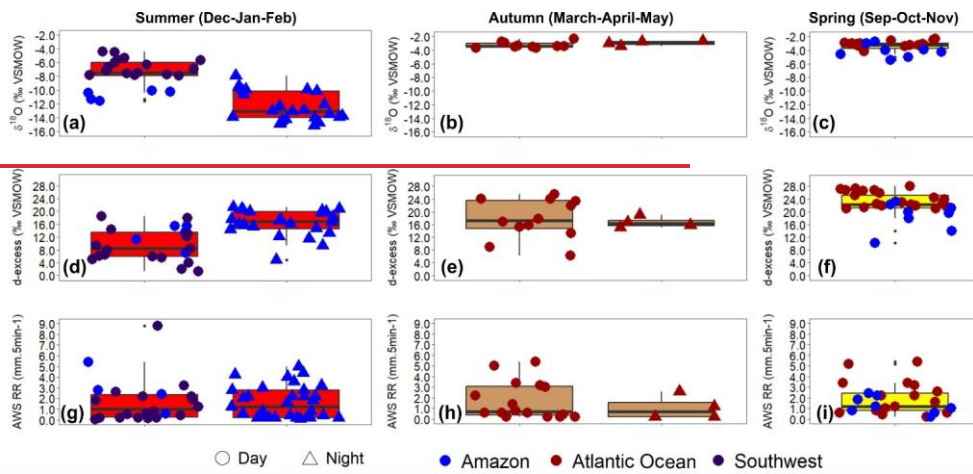
945 **Formatado:** Inglês (Reino Unido)



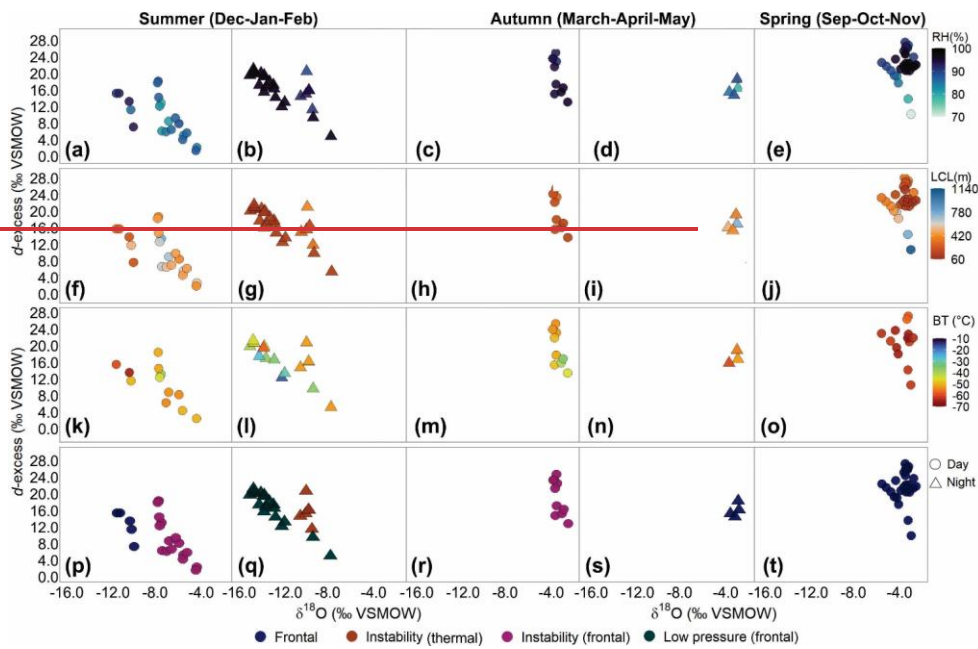


950 **Figure 2-2.** (a) Seasonal variation of $\delta^{18}\text{O}$ and d -excess values in monthly rainfall and aggregated monthly $\delta^{18}\text{O}$ values high-frequency convective rainfall sampling discussed in this study (b) AQUA/AIRS latent heat flux. (c) MERRA-2 outgoing longwave radiation (monthly averaged daytime and night-time data) (d) monthly rainfall amounts at Rio Claro separated into day and night fraction (no rainfall types distinguished). The star symbol indicates the collected high-frequency events, ranked according to average values of $\delta^{18}\text{O}$.

Formatado: Fonte: Negrito



955 **Figure 3.** (a, b, c) $\delta^{18}\text{O}$, (d, e, f) *d*-excess and (g, h, i) AWS rainfall rates in seasonal color-coded box-plots for summer (red), autumn (light brown) and spring (yellow), during day (circle) and night (triangle) time. Symbols are color-coded by the HYSPLIT derived origin of rain-producing air masses based on Fig. 1e: Amazon (blue), Atlantic Ocean (reddish-purple) and Southwest Brazil (dark-purple). Summer is defined as the period from December to February, autumn from March to April and spring from September to November.



960 **Figure 4.** (a, b, c) AWS RH, (d, e, f) LCL—lifting condensation level (meters), (g, h, i) GOES-16 BT—brightness temperature and (j, k, l) atmospheric systems with d -excess and $\delta^{18}\text{O}$ at daytime (circle) and night-time (triangle) for summer, autumn and spring seasons.

965

970

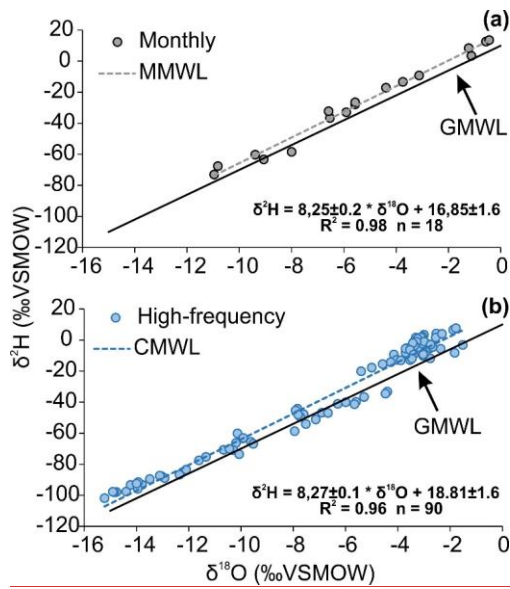


Figure 3. Table 1. Spearman rank correlations between isotopic composition of rainfall and meteorological parameters

Seasons		Summer				Autumn [§]		Spring	
		Day		Night		-	-	-	-
Isotopes		δ ¹⁸ O	d-excess	δ ¹⁸ O	d-excess	δ ¹⁸ O	d-excess	δ ¹⁸ O	d-excess
GOES	BT	0.43	-0.08	-0.25	-0.19	0.53	-0.08	0.14	-0.26
	Z	-0.38	-0.19	-0.14	0.32	0.34	-0.29	-0.22	0.55
MRR	w	-0.16	-0.26	-0.14	0.10	0.14	-0.19	-0.13	0.59
	LWC	-0.07	-0.35	-0.20	0.41	0.00	-0.11	-0.29	0.45
	RR	-0.52	-0.22	-0.40	0.37	0.00	0.00	-0.25	0.36
AWS	LCL	0.47	0.75	0.86	-0.68	-0.33	0.40	-0.42	-0.16
	Temp	-0.64	0.5	-0.22	0.11	-0.56	0.56	0.48	0.4
	RH	-0.51	-0.74	-0.86	0.68	0.30	-0.38	0.42	0.16
	RR	-0.57	-0.19	-0.34	0.41	0.16	0.00	-0.18	0.11

Formatado: Fonte: 10 pt, Inglês (Estados Unidos)

Formatado: Fonte: 10 pt, Itálico

Formatado: Fonte: 10 pt, Inglês (Estados Unidos)

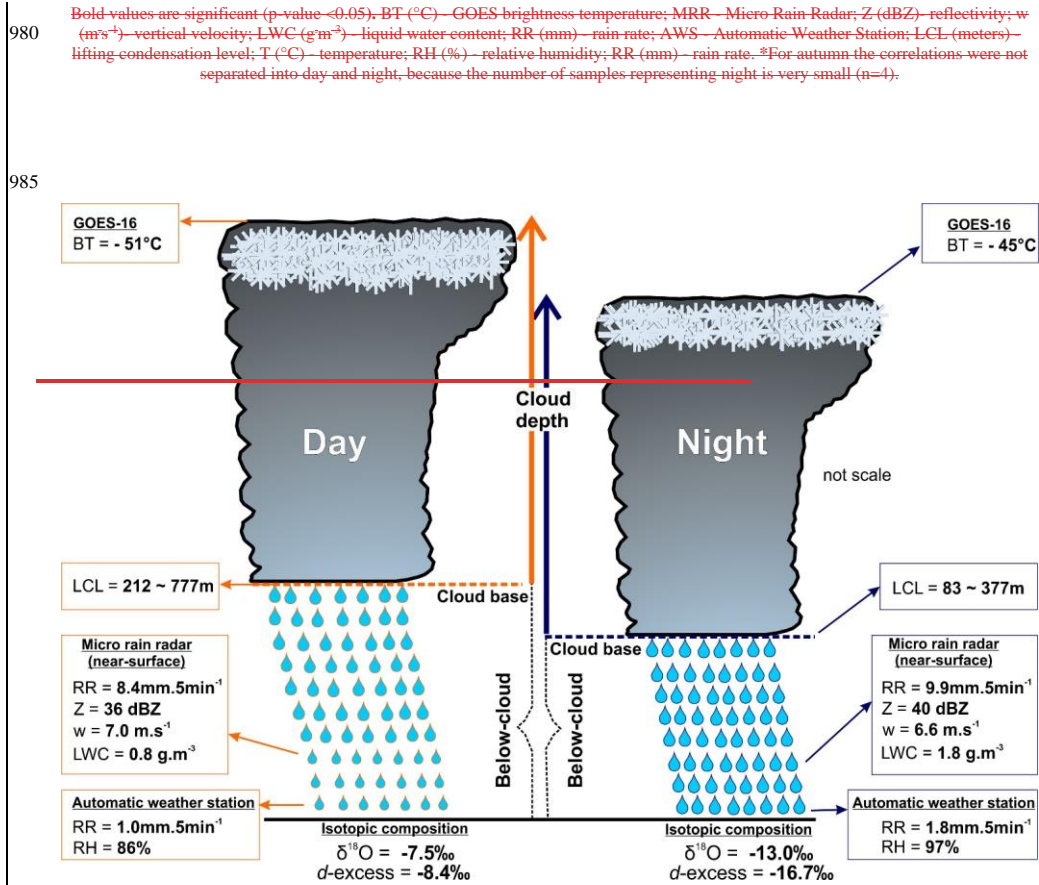
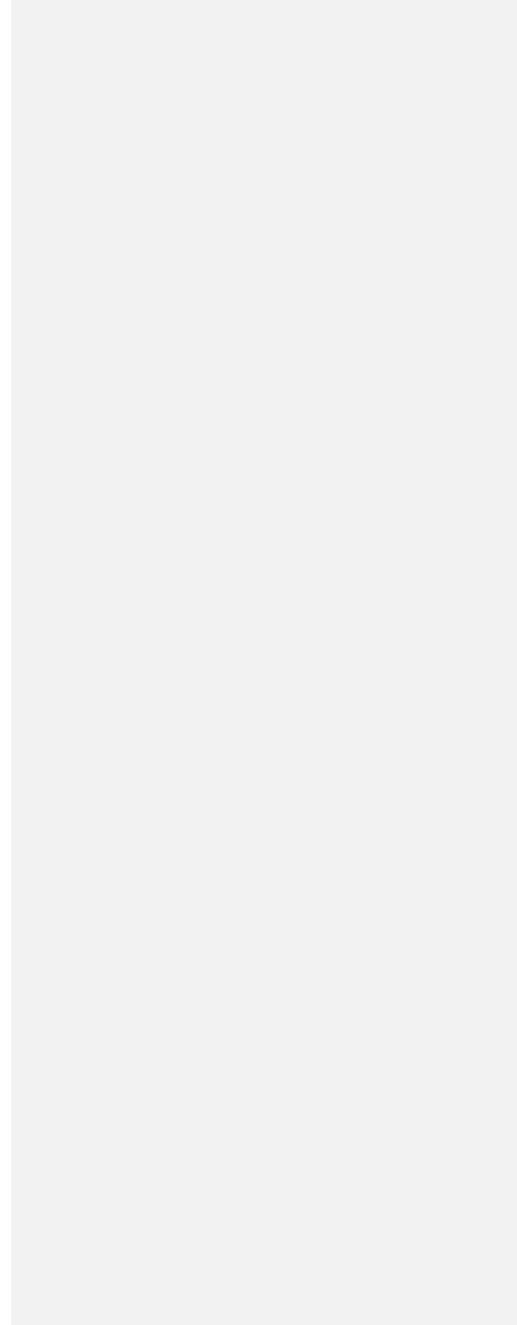


Figure 5. Schematic diagram for daytime (orange) and night-time (dark blue) situations of convective rainfall occurrences during summer at the inland tropics of Brazil. Vertical structure of convective cloud is characterized by the cloud depth (GOES-16 BT—brightness temperature $^{\circ}\text{C}$) and cloud-base (LCL—lifting condensation levels in meters). Below-cloud illustrate falling raindrops and their interactions with atmosphere near-surface (150m–350m) by Micro rain radar data, RR—rain rates, Z—reflectivity, w —fall velocity, LWC—liquid water content and at surface by Automatic weather station, RR—rain rates, ΔT —difference between maximum and minimum surface air temperature and RH—relative humidity. Differences in cloud structure and atmosphere below-cloud generate the differences in isotopic composition ($\delta^{18}\text{O}$ and d -excess) of convective rainfall observed. The illustration of cloud and raindrops are not scale.

1000



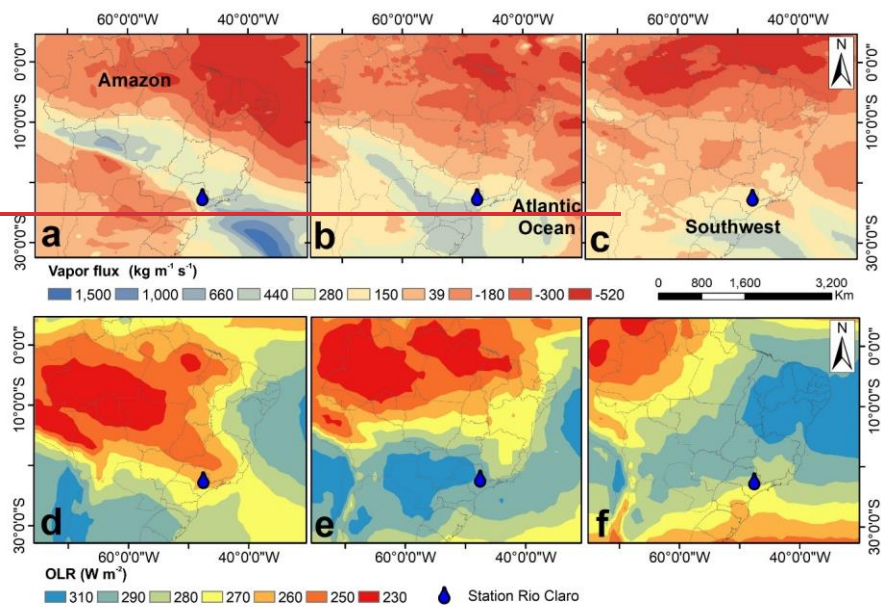


Figure 6. (a) Amazon, (b) Atlantic Ocean and (c) Southwest Brazil are HYSPLIT origin and were combined with ERA-5 vertical integral of eastward water vapor flux for the days when convective rainfall events occurred, during (d) summer, (e) autumn and (f) spring aggregated with MERRA-2 outgoing longwave radiation between 2019 and 2021. The position of the names indicates the origin of HYSPLIT trajectories. Positive values in Fig. a,b,c indicate the direction of moisture vapor flux from left to right, and negative values from right to left. Lower OLR (red) values indicate higher convective activity.

Appendices

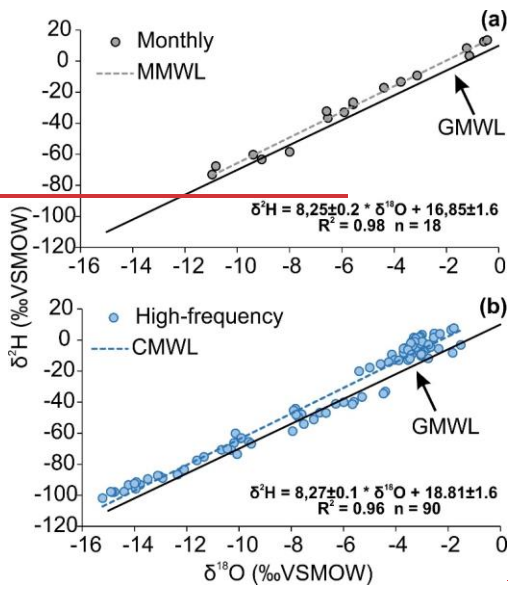
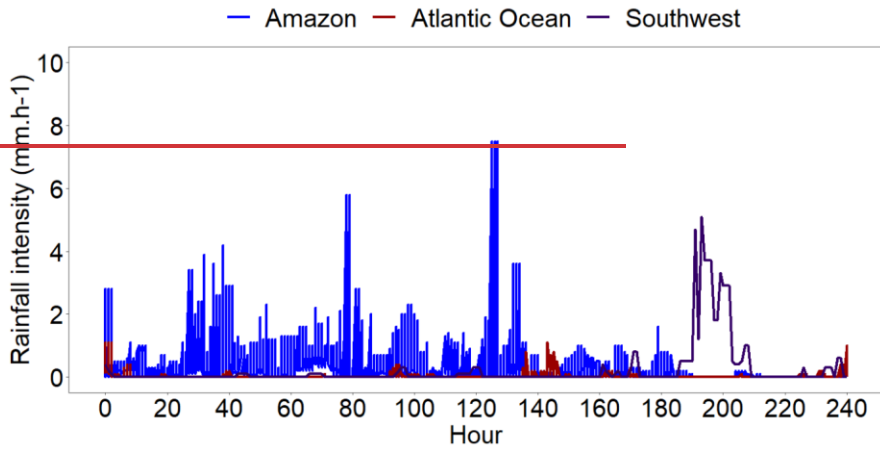


Figure A1. (a) Monthly and (b) high-frequency $\delta^2\text{H}$ and $\delta^{18}\text{O}$ rainfall data plotted in the $\delta^2\text{H}/\delta^{18}\text{O}$ space. LMWL – local meteoric water line based on monthly values, CMWL – convective meteoric water line and GMWL – global meteoric water line.

Formatado: Fonte: Negrito

Formatado: Centralizado



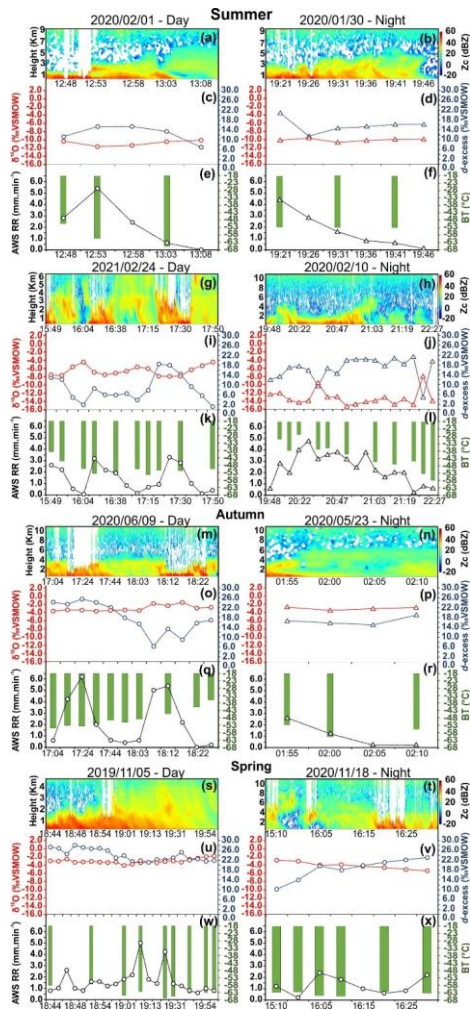


Figure A2. Rainfall intensity on HYSPLIT backward trajectories (240 hours) related to the moisture origin (Figure 1e) for all convective events. The Amazon trajectories reveal quasi-continuous rainout during pathway 4. Intra-event variability of moist air masses over the Amazon Basin down to the collection site at Rio Claro.

1030
1035
1040

Table B1. Meteorological data for eight convective rainfall sampling. For summer (day and night season, 2020/02/01 (a, c, e), 2020/01/30 (b, d, f), 24/02/21 (g, i, k) and 2020/02/10 (h, j, l), autumn (day-, 09/06/2020 (m, o, q) and night 23/05/2020 (n, p, r), autumn 05/11/2019 (s, u, w) and spring (day)

Formatado: Inglés (Estados Unidos)

Formatado: Inglés (Estados Unidos)

Formatado: Inglés (Estados Unidos)

Seasons		Summer						Autumn						Spring		
Meteorological data		Daytime			Night-time			Daytime			Night-time			-	-	-
		min	max	median	min	max	median	min	max	median	min	max	median	min	max	median
GOES	BT	-66	-39	-51	-57.8	-16.2	-45	-55	-36	-50	-61	-53	-56	-66.7	-57.3	-63
MRR	Z	20	51	36	0.93	46	40	17	51	42	22	44	33	24	50	45
	w	5.4	8.8	7.0	0.26	7.7	6.6	5.6	8.7	7.6	5.0	8.1	6.6	5.4	8.9	7.8
	LWC	0.0	14.0	0.8	0.03	7.6	1.8	0.1	3.8	1.2	0.1	3.3	1.0	0.0	4.0	2.1
AWS	RR	0.5	10.0	8.4	0.27	10.0	9.9	0.02	10	8.9	5.0	8.1	6.6	1.0	10	9
	LCL	212	777	452	83	377	95	133	340	167	355	757	449	65	1137	225
	Temp	19	25	21	20	24	22	18	20	19	18	20	19	19	27	21
	RH	79	94	86	89	98	97	90	96	95	78	89	86	71	98	93
HYSPLIT	RR	0.03	8.8	1.0	0.1	5.0	1.8	0.01	5.4	0.6	0.2	2.6	0.7	0.2	5.4	1.2
	Height	31	1110	1727	0	3212	778	1185	3576	2030	44	1500	287	0	11104	1781
	Rainfall	0.00	10.70	0.37	0.00	13.20	0.53	0.00	1.00	0.01	0.00	1.10	0.01	0.00	2.40	0.03

Bolded values were used to create the figure 5. BT (°C)—GOES18/11/2020 (t, v, x). $\delta^{18}\text{O}$ is red color. *d*-excess is orange, rain rate (RR) in dark blue, brightness temperature—MRR—(BT) in green. The Z_c is the corrected reflectivity of Micro Rain Radar; Z (dBZ)—reflectivity; w (m s⁻¹)—plotted as vertical velocity; LWC (g m⁻³)—liquid water content; RR (mm.5min⁻¹)—rain rate; AWS—Automatic Weather Station;

~~LCL (meters) — lifting condensation level; T (°C) — temperature; RH (%) — relative humidity; RR (mm.5min⁻¹) — rain rate. Meteorological values along HYSPLIT trajectories; (meters) height; RH (%) — relative humidity; Rainfall rate (mm.h⁻¹).~~

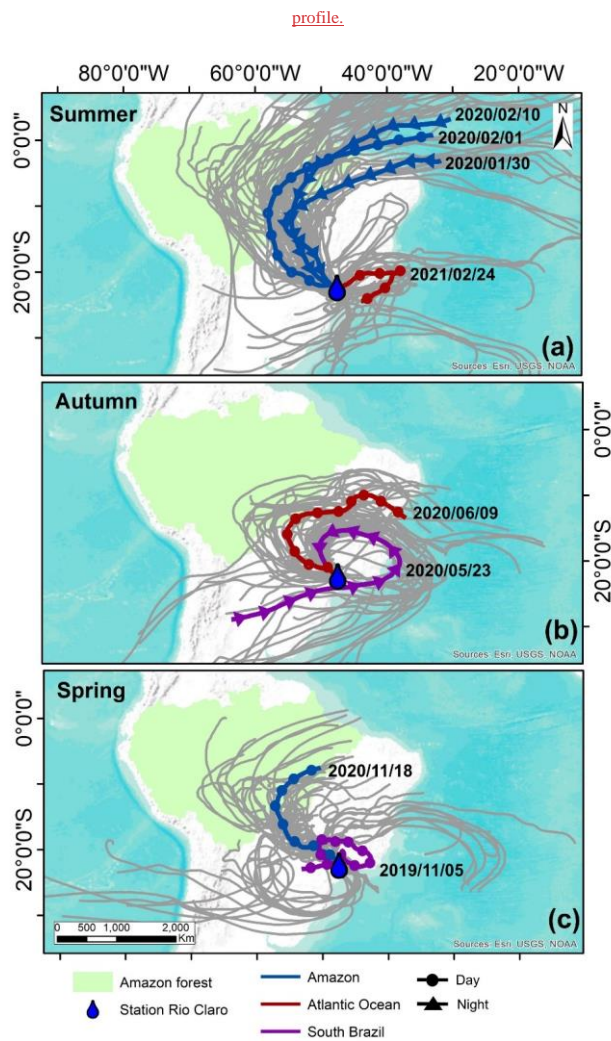


Figure 5. Ten-day backward trajectories arriving at Rio Claro station of eight convective events on (a) Summer, (b) Autumn and (c) Spring. Twenty-seven ensembles are grey lines, and the mean trajectory is the colored lines. The colors of the mean trajectories indicate the origin of air masses: blue influenced by Amazon Forest, Tuscan red from Atlantic Ocean and Purple from South Brazil portion.

Symbols are daytime of convective events, day (circle) and night (triangle). The authors used trivial information, the borders of the countries and the ocean provided by the ESRI base map.

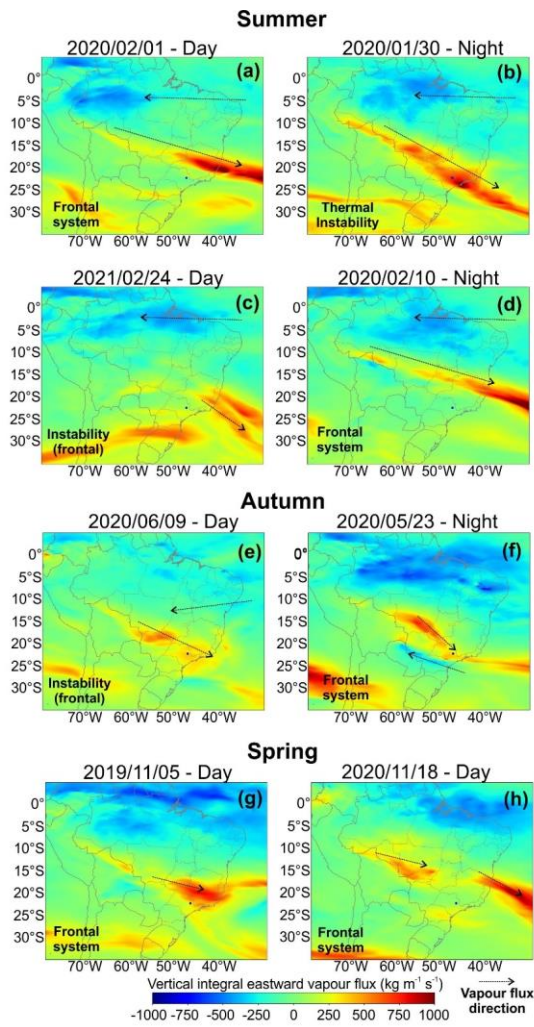


Figure 6. ERA-5 vertical integral of eastward water vapor flux for the days when convective rainfall events occurred, during (a, b, c, d) summer, (e, f) autumn and (g, h) spring aggregated with weather systems text. Positive values indicate the direction of moisture vapor flux

Formatado: Legenda, Centralizado

060 from left to right, and negative values from right to left. Arrows illustrate the direction of vapour flux. The weather systems are indicated for each rainfall event.